Renewable Energy 35 (2010) 1644–1661

Contents lists available at ScienceDirect

Renewable Energy

journal homepage: www.elsevier.com/locate/renene

Application of the time-dependent mild-slope equations for the simulation of wake effects in the lee of a farm of Wave Dragon wave energy converters

Charlotte Beels [a], Peter Troch [a,*], Kenneth De Visch [a], Jens Peter Kofoed [b], Griet De Backer [a]

[a] Ghent University, Department of Civil Engineering, Technologiepark 904, B-9052 Zwijnaarde, Belgium
[b] Aalborg University, Department of Civil Engineering, Sohngaardsholmsvej 57, DK-9000 Aalborg, Denmark

ARTICLE INFO

Article history:
Received 9 January 2009
Accepted 1 December 2009
Available online 16 February 2010

Keywords:
Wake
Farm
Porous structure
Mild-slope equations
Wave energy
Wave Dragon

ABSTRACT

Time-dependent mild-slope equations have been extensively used to compute wave transformations near coastal and offshore structures for more than 20 years. Recently the wave absorption characteristics of a Wave Energy Converter (abbreviated as WEC) of the overtopping type have been implemented in a time-dependent mild-slope equation model by using numerical sponge layers. In this paper the developed WEC implementation is applied to a single Wave Dragon WEC and multiple Wave Dragon WECs. The Wave Dragon WEC is a floating offshore converter of the overtopping type. Two wave reflectors focus the incident wave power towards a ramp. The focussed waves run up the ramp and overtop in a water reservoir above mean sea level. The obtained potential energy is converted into electricity when the stored water drains back to the sea through hydro turbines. The wave reflectors and the main body (ramp and reservoir) are simulated as porous structures, exhibiting the same reflection, respectively absorption characteristics as obtained for the prototype Wave Dragon WEC. The wake effects behind a single Wave Dragon WEC are studied in detail for uni- and multidirectional waves. The shadow zone indicating the wake effect is decreasing with increasing directional spreading. The wake in the lee of a farm of five Wave Dragon WECs, installed in a staggered grid (3 WECs in the first row and 2 WECs in the second row), is calculated for three in-between distances of respectively D, $2D$ and $3D$, with D the distance between the tips of the wave reflectors of a single WEC. As a result, a farm of five Wave Dragon WECs installed in a staggered grid with an in-between distance of $2D$ is preferred, when taking cost and spatial considerations into account.

1. Introduction

The increasing energy demand and the Kyoto agreement to reduce the greenhouse gas emissions, have renewed the interest in renewable energy. In the last decade many concepts for wave power conversion have been invented and tested. Two main principles of wave power conversion can be distinguished: (i) Wave Energy Converters (WECs) with a body or water column that is oscillating and consequently generating a wave that interferes destructively with the incident waves and (ii) WECs that capture the overtopped waves in a basin above mean sea level (Fig. 1) and consequently absorb a part of the incident wave power comparable to a porous structure. In this paper a WEC based on the second principle, the Wave Dragon WEC, is studied.

The Wave Dragon WEC is a floating offshore converter which consists of two main structural elements (Fig. 2):

- two wave reflectors to focus the incoming waves towards a double curved ramp;
- a main body where the focussed waves run up the curved ramp, overtop in a water reservoir above mean sea level and consequently have an increased potential energy compared to the surrounding sea. The reservoir contains a set of low head hydro turbines to convert the created potential energy into electricity when the water in the reservoir drains back to the sea through the turbines.

A lot of research has been carried out on the Wave Dragon WEC in order to:

- guarantee its survivability (control of forces on wave reflectors and mooring system) with special attention to the reflector joint [1],

* Corresponding author. Tel.: +32 9 264 54 89; fax: +32 9 264 58 37.
E-mail addresses: charlotte.beels@ugent.be (C. Beels), peter.troch@ugent.be (P. Troch), kenneth.devisch@ugent.be (K. De Visch), jpk@civil.aau.dk (J.P. Kofoed), griet.debacker@ugent.be (G. De Backer).

0960-1481/$ – see front matter © 2009 Elsevier Ltd. All rights reserved.
doi:10.1016/j.renene.2009.12.001

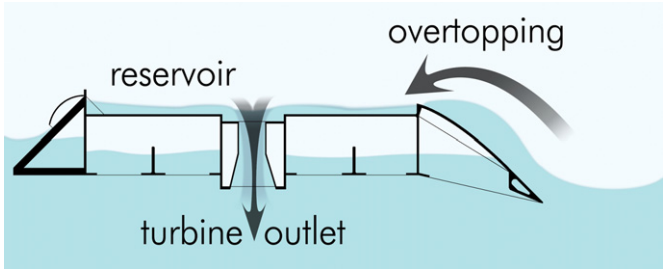

Fig. 1. Overtopping principle (copyright Wave Dragon).

- optimize the ramp profile [2], the wave reflectors [3,4] and the floating level [5] to increase wave overtopping,
- minimize motions [6],
- develop efficient and robust turbines for an extremely low and varying head [7],
- optimize the speed of the turbines [8] and the time to switch on or switch off the turbines [5] to maximize power production,
- and finally reduce costs.

A detailed overview of previous research on the Wave Dragon WEC is given in Kofoed et al. and Tedd et al. [9,10].

The testing of a 1:4.5 scale prototype (relative to the device developed for a North Sea wave climate with a mean wave power of 24 kW/m) of the Wave Dragon WEC in Nissum Bredning (Denmark) from 2002 till 2005 has resulted in a power matrix [11]. This power matrix shows the produced power as a function of the wave conditions (peak wave period T_p and significant wave height H_s). The power production of a single Wave Dragon WEC in a 24 kW/m wave climate is limited to 4 MW. To produce amounts of power comparable to a classic power plant, several Wave Dragon WECs need to be arranged in a geometric configuration or 'farm'. Wave Dragon WECs in a farm are partly absorbing, partly redistributing the incident wave power. Consequently the power absorption of each individual Wave Dragon WEC in a farm is affected by its neighbouring Wave Dragon WECs. The local wave climate determines the performance of each Wave Dragon WEC in the farm.

In this paper the total power absorbed by a farm of five Wave Dragon WECs (placed in a staggered grid) is studied for different in-between distances in a phase-resolving time domain model based on the mild-slope equations of Radder and Dingemans [12], MILDwave, developed at Ghent University. Moreover, the wave height reduction behind an isolated Wave Dragon WEC and a farm of Wave Dragon WECs is estimated. The results can be easily extended for larger farms.

The possibility to model a single WEC and a farm of WECs of the overtopping type in the linear mild-slope wave propagation model MILDwave has previously been studied by Beels et al. [13]. The generic approach described in Beels et al. is applied to the Wave Dragon WEC in this paper.

In the next section the basic equations for wave generation and propagation in the mild-slope equation model MILDwave are briefly described. Furthermore the technique to implement a WEC of the overtopping type in MILDwave, is summarized. Section 3 gives a detailed overview of the implementation of the Wave Dragon WEC in MILDwave. Moreover the wake effects in the lee of a single Wave Dragon WEC are studied for uni- and multidirectional waves. Section 4 deals with a farm of five Wave Dragon WECs. The total power absorption and wave height reduction behind the farm are calculated for different lay-outs in order to select an optimal farm lay-out. Finally in Section 5 the power absorption of five Wave Dragon WECs, installed in the selected farm lay-out, is estimated.

2. Mild-slope wave propagation model MILDwave

2.1. Wave generation and propagation

The depth-integrated mild-slope equations of Radder and Dingemans (1985) [12], which describe the transformation of linear irregular waves with a narrow frequency band over a mildly varying bathymetry (bed steepness up to 1/3 [14]), are given in equations (1) and (2):

$$\frac{\partial \eta}{\partial t} = B\phi - \nabla(A\nabla\phi) \tag{1}$$

$$\frac{\partial \phi}{\partial t} = -g\eta \tag{2}$$

where η and ϕ are respectively the surface elevation and velocity potential at the free water surface, ∇ is the horizontal gradient

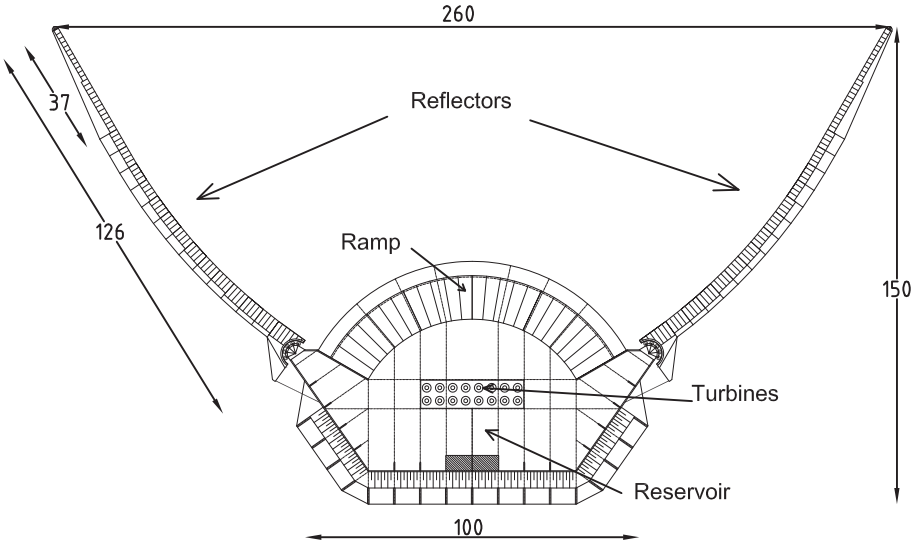

Fig. 2. Main structural elements of a Wave Dragon WEC (copyright Wave Dragon) – dimensions in m.

operator, t is the time, g is the gravitational acceleration and where B and A are defined as:

$$B = \frac{\overline{\omega}^2 - \overline{k}^2\overline{C}\overline{C}_g}{g} \tag{3}$$

$$A = \frac{\overline{C}\overline{C}_g}{g} \tag{4}$$

with the phase velocity $\overline{C}$ and the group velocity $\overline{C}_g$ for a wave with carrier wave number $\overline{k}(= 2\pi/\overline{L})$, carrier angular frequency $\overline{\omega}(= 2\pi\overline{f})$, carrier wave length $\overline{L}$ and carrier frequency $\overline{f}$. Overbar ($^-$) denotes that the wave characteristic is calculated for the carrier frequency. MILDwave simulates wave transformation processes such as refraction, shoaling, reflection, transmission and diffraction, intrinsically. Energy dissipation by bottom friction and wave breaking is not taken into account.

In MILDwave waves are generated at the offshore boundary by using the source term addition method, i.e. by adding an additional surface elevation η^* to the calculated value on a wave generation line for each time step given by equation (5) [15]:

$$\eta^* = 2\eta_i \frac{C_e \Delta t}{\Delta y} \sin\theta \tag{5}$$

with the water surface elevation of incident waves η_i, the angle of wave rays from the x-axis θ ($0^\circ \le \theta \le 180^\circ$), the grid size in y-direction Δy, the time step Δt and the energy velocity C_e given by equation (6):

$$C_e = \overline{C}_g \frac{\overline{\omega}}{\omega} \sqrt{1 + \frac{\overline{C}}{\overline{C}_g}\left(\left(\frac{\omega}{\overline{\omega}}\right)^2 - 1\right)} \tag{6}$$

The wave generation line is assumed to be parallel to the x-axis in equation (5) (Fig. 3). It has been proven that the model of Radder and Dingemans can be used to simulate the transformation of uni- and multidirectional random waves [15]. For the generation of random waves, the peak frequency is used as a carrier frequency in equations (3) and (4) as the peak frequency is usually lower than the weight-averaged frequency and as the dispersion relation of the

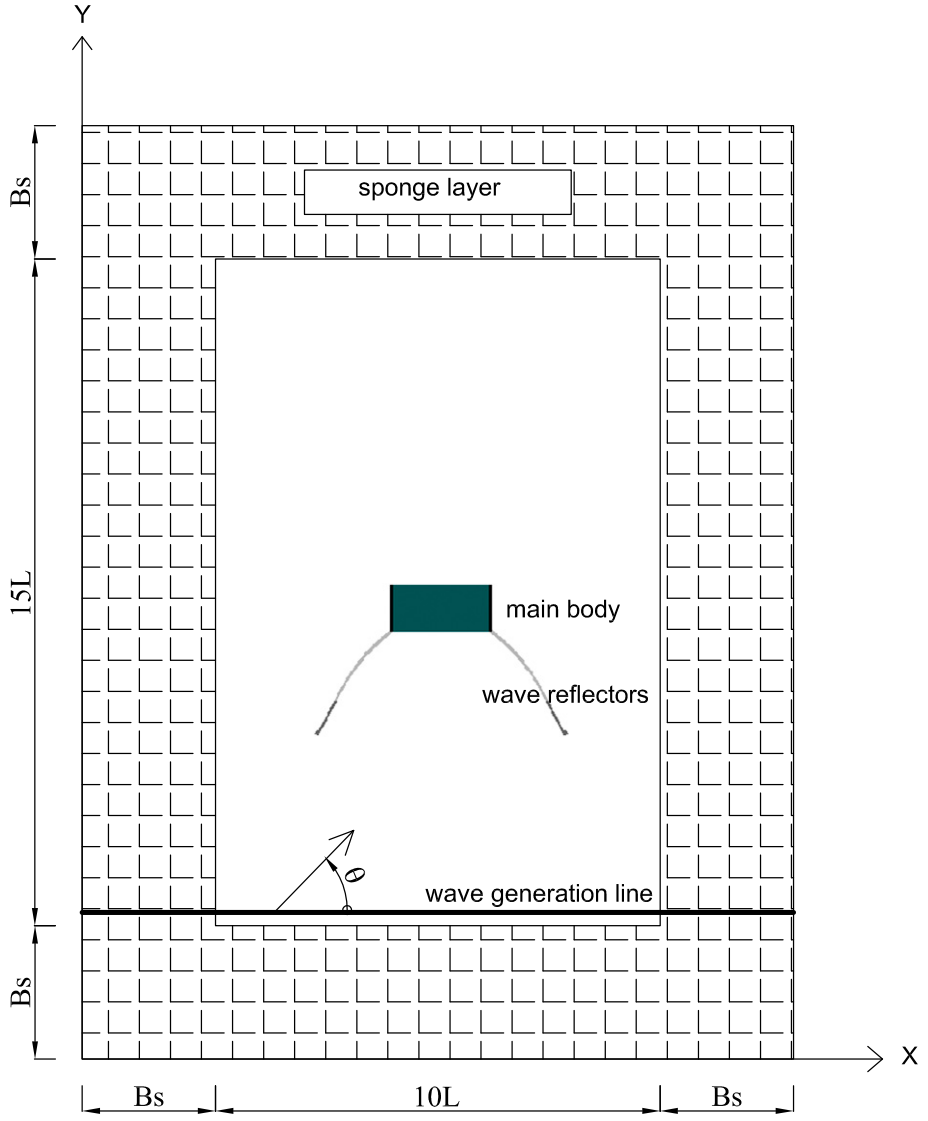

Fig. 3. Definition sketch of wave basin with a Wave Dragon WEC in plan view for generation of unidirectional waves.

model of Radder and Dingemans is more accurate in the high frequency range [15,16]. For unidirectional irregular waves equation (5) can be written as equation (7) by using a single summation model:

$$\eta^* = 2\sum_{n=1}^{N}\sqrt{2S(f_n)\Delta f}\sin(k_n x\cos\theta + k_n y\sin\theta - \omega_n t + \phi_n)\frac{C_{e,n}\Delta t}{\Delta x}\sin\theta \tag{7}$$

with the angular frequency $\omega_n = 2\pi f_n = 2\pi(n-1)\Delta f + 2\pi f_{\min}$, the frequency interval $\Delta f = f_{\max} - f_{\min}/N - 1$ and the random phase ϕ_n.

A parameterised JONSWAP spectrum (equation (8)) is used as an input spectrum [17]:

$$S(f_n) = \frac{0.0624}{0.230 + 0.0336\gamma - \left(\frac{0.185}{1.9+\gamma}\right)} H_s^2 f_p^4 f_n^{-5}\gamma^{\exp\left(-\frac{(f_n-f_p)^2}{2\sigma^2 f_p^2}\right)} \times \exp\left(\frac{-5}{4}\left(\frac{f_p}{f_n}\right)^4\right) \tag{8}$$

with the significant wave height H_s, the peak frequency f_p, the peak enhancement factor γ and the spectral width parameter σ which equals 0.07 for $f_n \le f_p$ and 0.09 for $f_n \ge f_p$.

To generate multidirectional random waves the set-up in Fig. 3 cannot be applied as not all wave components are travelling in the same direction. Recently Lee and Yoon [18] developed a method for internally generating multidirectional waves on an arc in a rectangular grid system using the source term addition method (Fig. 4). This technique generates wave energy much closer to the target energy than the technique of generating waves on three wave generation lines [15], especially for a small grid size. The grid point nearest to the arc is used as a wave generation point. Depending on the angle of the wave generation arc with the x-axis, respectively y-axis the additional surface elevation is given by:

$$\eta^* = \begin{cases} 2\eta_i\dfrac{C_e\Delta t}{\Delta x}\dfrac{(-\cos(\epsilon+\theta))}{\cos\epsilon} & \text{case 1} \\ 2\eta_i\dfrac{C_e\Delta t}{\Delta y}\dfrac{(-\sin(\epsilon-\theta))}{\cos\epsilon} & \text{case 2} \\ 2\eta_i\dfrac{C_e\Delta t}{\Delta y}\dfrac{\sin(\epsilon+\theta)}{\cos\epsilon} & \text{case 3} \\ 2\eta_i\dfrac{C_e\Delta t}{\Delta x}\dfrac{\cos(\epsilon-\theta)}{\cos\epsilon} & \text{case 4} \end{cases} \tag{9}$$

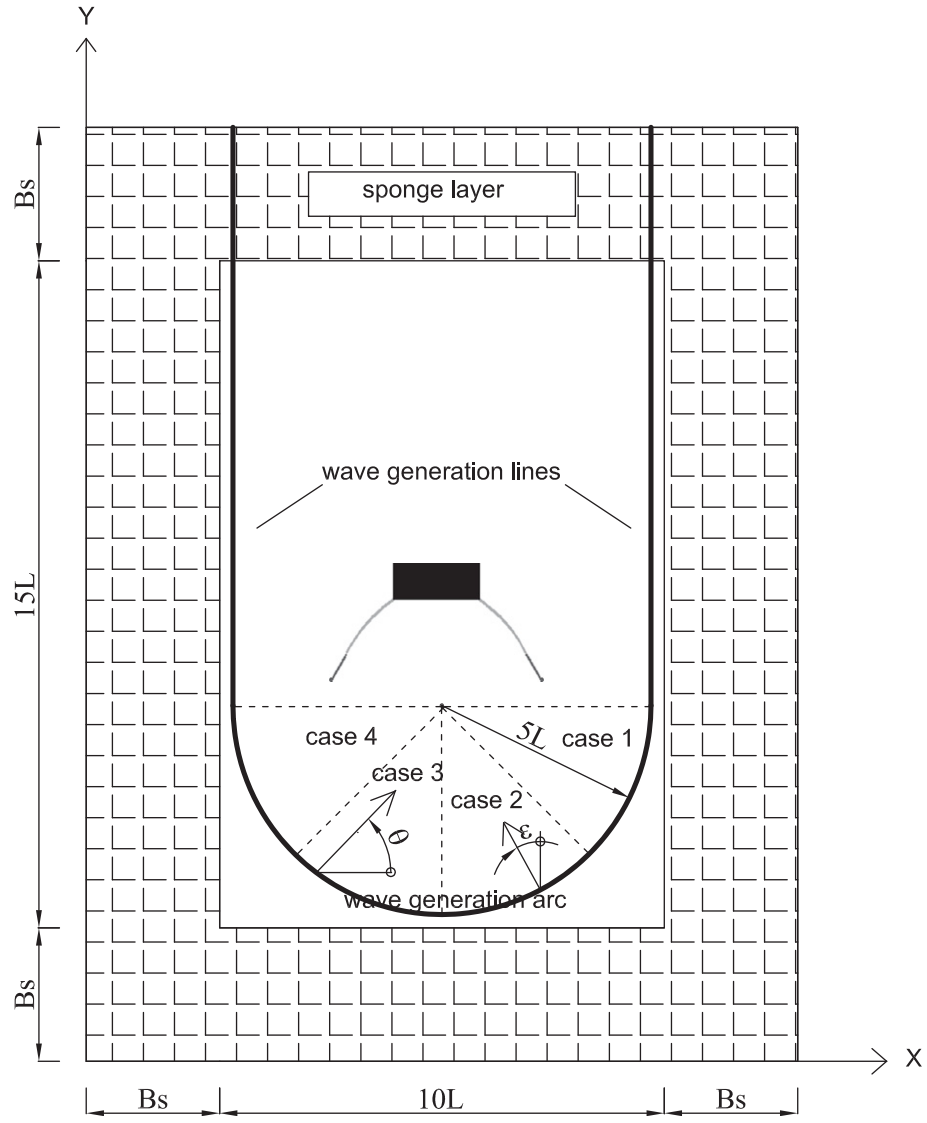

Fig. 4. Definition sketch of wave basin with a Wave Dragon WEC in plan view for generation of multidirectional waves.

with ϵ the angle between the line normal to the wave generation curve and the x-axis for case 1 and 4, respectively y-axis for case 2 and 3. ϵ is indicated on Fig. 4 for case 2.

On the left, respectively right generation line, the additional surface elevation is given by equations (10) and (11):

$$\eta^* = 2\eta_i \frac{C_e \Delta t}{\Delta x} \cos\theta \tag{10}$$

$$\eta^* = 2\eta_i \frac{C_e \Delta t}{\Delta x} (-\cos\theta) \tag{11}$$

When the wave direction is not pointing to the inner domain on a part of the wave generation arc or on one of the wave generation lines, no waves are generated in those cells. For example when $\theta = 45^\circ$ no waves are generated on the right generation line and on the first part of the arc (case 1).

A single summation model is implemented to generate short-crested waves [19]. In the latter model each wave component has a unique frequency while several wave components are travelling in the same direction. The value of the additional surface elevation on the left wave generation line parallel with the y-axis, η^*, is expressed by equation (12) with the single summation model:

$$\begin{aligned}\eta^* = 2 \sum_{n=1}^{N} \sum_{m=1}^{M} & \sqrt{2S(f_{nm}) D(f_{nm}, \theta_m) M \Delta f \Delta\theta} \\ & \times \sin(k_{nm} x \cos\theta_m + k_{nm} y \sin\theta_m - \omega_{nm} t + \phi_{nm}) \\ & \times \frac{C_{e,nm} \Delta t}{\Delta x} \cos\theta_m \end{aligned} \tag{12}$$

with the angular frequency $\omega_{nm} = 2\pi f_{nm} = 2\pi[M(n-1)+m]\Delta f + 2\pi f_{min}$, the frequency interval $\Delta f = f_{max} - f_{min}/(NM) - 1$, the wave propagation angle $\theta_m = (m-1)\Delta\theta + \theta_o - \theta_{max}$, the angle interval $\Delta\theta = 2\theta_{max}/M - 1$, the random phase ϕ_{nm} and the directional spreading function $D(f_{nm}, \theta_m)$ [20]:

$$D(f_{nm}, \theta_m) = \frac{2^{2s-1}}{\pi} \frac{\Gamma^2(s+1)}{\Gamma(2s+1)} \cos^{2s}\left(\frac{\theta_m - \theta_o}{2}\right) \tag{13}$$

with θ_o the mean wave angle. The directional spreading parameter s gives the degree of directional energy concentration. For wind seas (like the North Sea), the spectrum is rather broad and the value of s is rather low. The parameter s can be related to the frequency by equation (14) [21]:

$$s = \begin{cases} (f_{nm}/f_p)^5 s_{max} : f_{nm} \le f_p \\ (f_{nm}/f_p)^{-2.5} s_{max} : f_{nm} \ge f_p \end{cases} \tag{14}$$

The parameter s_{max} is the maximum value of the spreading parameter. Fixed values for s_{max} are given in equation (15) for wind and swell waves [21]:

$$s_{max} = \begin{cases} 10 : \text{wind waves} \\ 25 : \text{swell with short decay distance} \\ 75 : \text{swell with long decay distance} \end{cases} \tag{15}$$

Equation (16) gives the relation between the directional spreading parameter s and the standard deviation σ_θ, which is called the directional width [22]:

$$\sigma_\theta = \sqrt{\frac{2}{s+1}} \tag{16}$$

The effect of the fully reflective domain boundaries in MILDwave is negligible because absorbing sponge layers [23] at the outside boundaries (Figs. 3 and 4) are significantly dissipating the incoming wave energy by multiplying the calculated surface elevations on each new time step with an absorption function $S(b)$ (reflection coefficient smaller than 5% for $\mu = 1.04$ and $a_n = 60$ in equation (17)):

$$S(b) = \frac{1}{\exp\left((\mu^{-b} - \mu^{-B_s}) \ln a_n\right)} \tag{17}$$

with the length of the sponge layer B_s and the distance from the outside boundary b, both expressed in number of cells. In general a length of $2.5L_{max}$ [15], where L_{max} is the maximum wave length resulting from the cut-off incident frequency spectrum, is sufficient.

A finite difference scheme, as described in Brorsen and Helm-Petersen [24], is used to solve equations (1) and (2). The domain is divided in grid cells (uniform grid) with dimensions Δx and Δy and central differences are used for spatial as well as time derivates. The grid spacing $\Delta x = \Delta y$ is chosen so that $L_{min}/20 \le \Delta x = \Delta y \le L_{min}/10$ (L_{min} = shortest wave length (maximum frequency)) and the time step meets the Courant–Friedrichs–Lewy criterion, $\Delta t \le \Delta x / C_{max}$, to guarantee a stable and consistent result (C_{max} = maximum phase velocity).

Wave generation starts from quiescent water conditions at $t = 0$. A slow start of wave generation is obtained by multiplying the wave generation by $\tanh(0.5t/\overline{T})$, with the carrier wave period $\overline{T}$ [25]. Each time step, η and ϕ are calculated in the centre of each grid cell. Consequently waves are gradually propagating through the domain.

2.2. Sponge layer technique

A Wave Dragon WEC, installed in sea, is interacting with the incoming waves. The incident waves are partly overtopping in the reservoir and consequently absorbed. The other part is reflected on the WEC or transmitted under the WEC or diffracted around the structure. Therefore the Wave Dragon WEC is only absorbing a certain amount of the incident wave power available over the width of the device.

In Beels et al. [13] a WEC is implemented as an array of cells (covering the spatial extensions of the WEC) that have been assigned a given degree of absorption using the sponge layer technique. Absorption functions $S(x)$ or $S(y)$ define the absorption coefficient S attached to each cell of the WEC in x-direction, respectively y-direction (Fig. 3). By changing the values of the absorption coefficients or the number of absorbing cells, the degree of reflection and transmission and consequently absorption of the porous structure (WEC) can be changed. When all cells have a constant absorption coefficient $S(x) = S(y) = 0$, respectively 1, all incident wave power is reflected, respectively transmitted. A structure with a value of S equal to 0 represents a fully reflective structure. Cells with S equal to 1 are water cells. When the absorption coefficient is varying between 0 and 1, the incident waves are partly reflected, absorbed and transmitted. When assuming a constant absorption coefficient S for all cells of the WEC, the amounts of reflection, transmission and absorption are coupled. To avoid this coupling, the shape of the absorption function $S(y)$ through the WEC (when the direction of wave propagation = y-direction) is changed. This way the degree of absorption (and consequently transmission) can be tuned for a fixed amount of reflection on the WEC as specified by the developer.

To tune the reflection, transmission and consequently absorption characteristics of a WEC a structure composed of a series of absorbing cells is implemented in a numerical test flume (Fig. 5). The structure has a length equal to the length of the WEC and a width equal to the wave flume width.

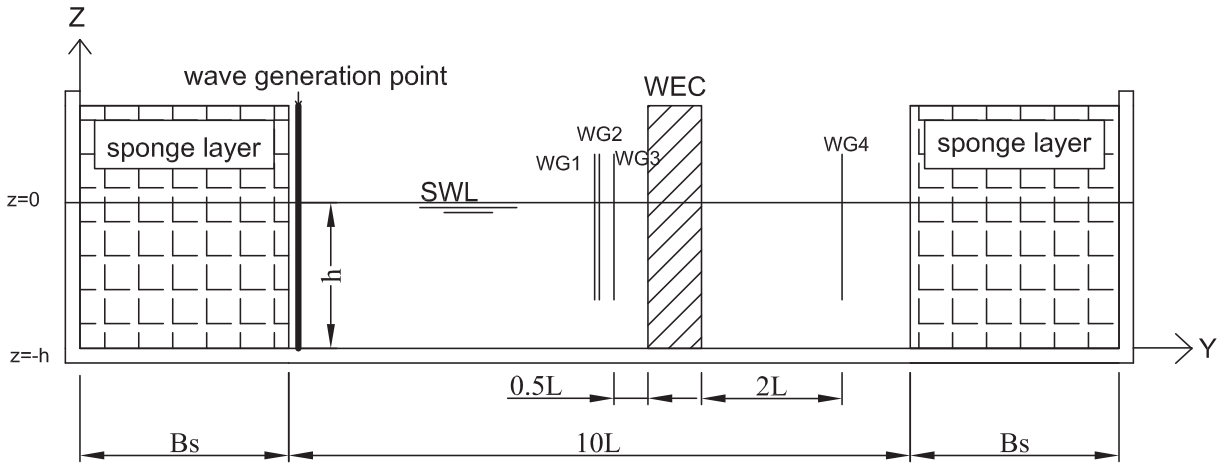

Fig. 5. Definition sketch of numerical test flume – cross section.

To determine the amount of reflection on and transmission through the absorbing structure, four wave gauges (WG) are placed in the wave flume (Fig. 5). Three wave gauges are installed half a wave length in front of the structure to measure the incident significant wave height $H_{s,\,i}$ and the reflected significant wave height $H_{s,\,r}$. The distances between the wave gauges are derived using Mansard and Funke's criteria [26] in order to perform a reflection analysis. One wave gauge is placed two wave lengths behind the WEC to measure the transmitted significant wave height $H_{s,\,t}$. The degree of absorbed power P_a/P_i in deep water is calculated from (conservation of energy):

$$\frac{P_a}{P_i} = 1 - K_r^2 - K_t^2 \tag{18}$$

with the wave power absorbed by the WEC P_a (W), the incident wave power over the width of the WEC P_i (W), the reflection coefficient $K_r = H_{s,r}/H_{s,i}$ and the transmission coefficient $K_t = H_{s,t}/H_{s,i}$.

3. Numerical study of a single Wave Dragon WEC

3.1. Test conditions

In this paper a Wave Dragon WEC with a rated power of 4 MW, in a typical North Sea wave climate (Location Ekofisk – 24 kW/m [27]), is studied. The dimensions of the Wave Dragon WEC are shown in Fig. 2. Wave situations in the North Sea [27] for significant wave heights between 0.5 m and 5.5 m and their related wave power (assuming a parameterized JONSWAP spectrum with $\gamma = 3.3$ and deep water) and frequency of occurrence are given in Table 1. During the rest of the year (frequency of occurrence = 10%), wave heights are mainly smaller than 0.5 m and sometimes larger than 5.5 m. These situations are neglected in the following, as they contribute only marginally to the total power production over a year. The mean wave power of the 5 considered wave situations is approximately 17 kW/m. Waves with a significant wave height H_s = 1 m and peak wave period T_p = 5.6 s have the highest frequency of occurrence (43%).

In all simulations 50 frequency components are used to generate approximately 500 irregular long-crested waves with a time step of 0.1 s and 0.05 s for T_p = 5.6 s and T_p = 7 s, 8.4 s, 9.8 s, 11.2 s, respectively (cell dimensions of 1 m for all wave periods). For the generation of short-crested waves (1000 waves) the number of frequency components is reduced to 20. A uniform deep water depth h (= 200 m) is used to avoid energy dissipation due to bottom friction and wave breaking.

Table 1
Wave situations in the North Sea (Location Ekofisk: distance to shore = 300 km, water depth = 71 m[27]).

H_s m	T_p s	Incident wave power p_i kW/m	Frequency of occurrence %
1	5.6	2.5	43
2	7.0	12.4	25
3	8.4	33.5	12
4	9.8	69.6	6
5	11.2	124.2	4

3.2. Implementation of a wave dragon WEC

The Wave Dragon WEC consists of 2 main structural elements with a different functioning (Fig. 6): (i) wave reflectors (subscript R) which reflect part of the incident wave power p_i towards the main body $p_{R,\,r}$ and (ii) a main body (subscript B) which is absorbing as much wave power as possible $P_{cs,\,B,\,a}$. The wave reflectors partly reflect the incident wave power p_i to increase the available wave power in front of the main body $P_{cs,\,R,\,i}$. They do not absorb wave power. The remaining incident wave power (i.e. not reflected part) is transmitted under the wave reflectors $p_{R,\,t}$. The increased wave

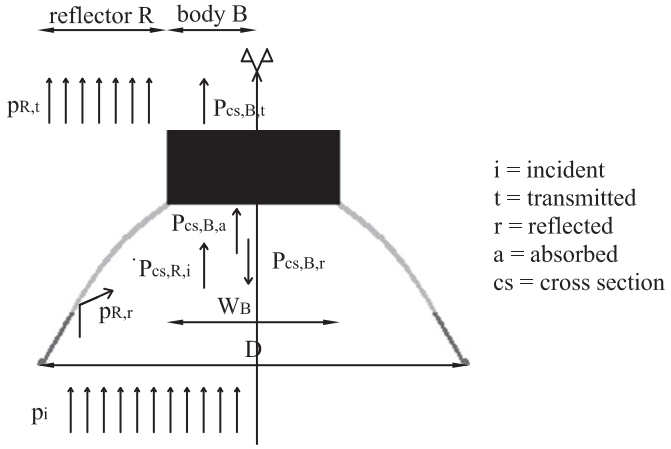

Fig. 6. Definition sketch of reflection on and transmission under the wave reflector and reflection on, transmission under and absorption by the main body – plan view.

power in front of the main body $P_{cs,\,R,\,i}$ is not completely absorbed by the main body, but is partly lost by transmission under the main body $P_{cs,\,B,\,t}$ and by reflection on the curved ramp $P_{cs,\,B,\,r}$.

Therefore the implementation of a Wave Dragon WEC in MILDwave is carried out in two phases: implementation of (i) wave reflectors and (ii) main body. Definition sketches of all relevant physical processes are given in Figs. 6 and 7. The used subscript abbreviations are also explained in these figures.

3.2.1. Implementation of the wave reflectors

The initial design of the wave reflectors has been evaluated by Nielsen and Kofoed [3] in a time-dependent mild-slope equation model. In Kramer and Frigaard [4] the geometry of the wave reflectors of the Wave Dragon WEC has been optimised by using a 3D boundary element method based on potential flow. The method has been validated through physical experiments in the 3D wave basin at Aalborg University (scale 1/50). The efficiency of each design of the wave reflectors, η_R^{target}, has been calculated by dividing the total wave power available in the cross section between the two reflectors $P_{cs,\,R,\,i}$ (W) when the wave reflectors are present, as indicated with a bold line on Fig. 8, by the total wave power of the undisturbed incident wave in the same cross section when no reflectors are present in the wave field $P_{cs,\,i}$ (W). No other parts than the wave reflectors were present in the wave field. The resulting efficiencies η_R^{target} [4] for the test conditions specified in this paper and the reflector lay-out applied in the 4 MW-type Wave Dragon WEC are given in Table 2. These target efficiencies are used during the implementation of the wave reflectors in MILDwave. The yearly averaged efficiency of the wave reflectors in a North Sea wave climate is approximately 130–140%. The efficiency increases for waves with a higher frequency. In general, waves with a higher wave frequency have a smaller wave height. Consequently the smaller incident significant wave heights are sufficiently increased by the wave reflectors to make wave overtopping possible. It is clear that the wave reflectors increase the frequency bandwidth of the Wave Dragon WEC.

The draft of the wave reflectors d_R differs along the length of the reflector. The draft decreases from approximately 8 m over a length of 89 m near the main body (indicated in light grey on Fig. 6) to 6 m at the tip of the reflector over a length of 37 m (indicated in dark grey on Fig. 6). As a consequence the transmission increases towards the tip of the reflector. As the equations in MILDwave are depth-integrated, the difference in draft is taken into account through the absorption coefficients of the cells of the reflectors. The absorption coefficient at the tips should be closer to 1 (larger amount of transmission) compared to the coefficient near the main body. The amounts of transmitted wave power under both parts of the wave reflector (with a draft d_R equal to 6 m and 8 m respectively) $p_{R,\,t}$ (W/m) are derived by assuming that all wave power below the draft of the wave reflector is transmitted (Fig. 7). The ratio between the time averaged (over one period) amount of energy flux integrated from the draft of the reflector up to the surface, p_{d_R} (W/m), and the time averaged amount of incident energy flux integrated from the seabed up to the surface or incident wave power, p_i (W/m), is given by equation (19) [2]:

$$\lambda_{d_R} = \frac{p_{d_R}}{p_i} = 1 - \frac{\sinh\left(2\,\mathrm{kh}\left(1-\frac{d_R}{h}\right)\right) + 2\,\mathrm{kh}\left(1-\frac{d_R}{h}\right)}{\sinh(2\,\mathrm{kh}) + 2\,\mathrm{kh}} \tag{19}$$

Consequently the amount of transmitted wave power under the wave reflectors is equal to $p_{R,t} = p_i - p_{d_R} = p_i(1 - p_{d_R}/p_i) = p_i(1-\lambda_{d_R})$. The ratio between the transmitted wave power under the wave reflectors and the incident wave power $p_{R,t}/p_i = (1-\lambda_{d_R})$ increases with increasing wave period and decreasing draft, as shown on Fig. 9.

In MILDwave the wave reflectors are assumed to be fixed, which is rather conservative, as small movements of the wave reflectors will increase the amount of transmission, which will blur the shadow zone in the lee of the Wave Dragon WEC. By using the efficiency of the wave reflectors (Table 2) and the amounts of transmission under the wave reflectors (Fig. 9), the reflectors are modelled in MILDwave using the sponge layer technique. The wave reflectors (without main body) are implemented in a numerical wave basin as shown in Fig. 8.

The values of the absorption coefficients of the cells of the wave reflectors, to obtain the target efficiency in the cross section (Table 2), are determined through an iterative approach. The total wave power available in the cross section between the wave reflectors when the reflectors are present, as indicated on Fig. 8 with $W_B = 100$ m, $P_{cs,\,R,\,i}$, is calculated by summation of the wave power in each cell of that section (with cell size $\Delta x = 1$ m):

$$P_{cs,R,i} = \sum_{k=1}^{100} \frac{\rho g^2}{64\pi} H_{s,k}^2 T_{e,k} \tag{20}$$

where ρ is the density of sea water and $T_e = m_{-1}/m_0$, is the energy period with m_n the *nth* moment of spectral density.

Finally the total wave power in the cross section between the wave reflectors $P_{cs,\,R,\,i}$ is divided by the wave power in the undisturbed wave in the same section $P_{cs,\,i} = W_B p_i$, with $W_B = 100$ m and p_i given in Table 1, to obtain the efficiency of the wave reflectors in the numerical model η_R^{num}.

The target efficiency η_R^{target} is obtained with several combinations of absorption coefficients. To select the best combination the amount of transmitted wave power below the wave reflectors $p_{R,\,t}$ is determined. Therefore both parts of the wave reflectors, with

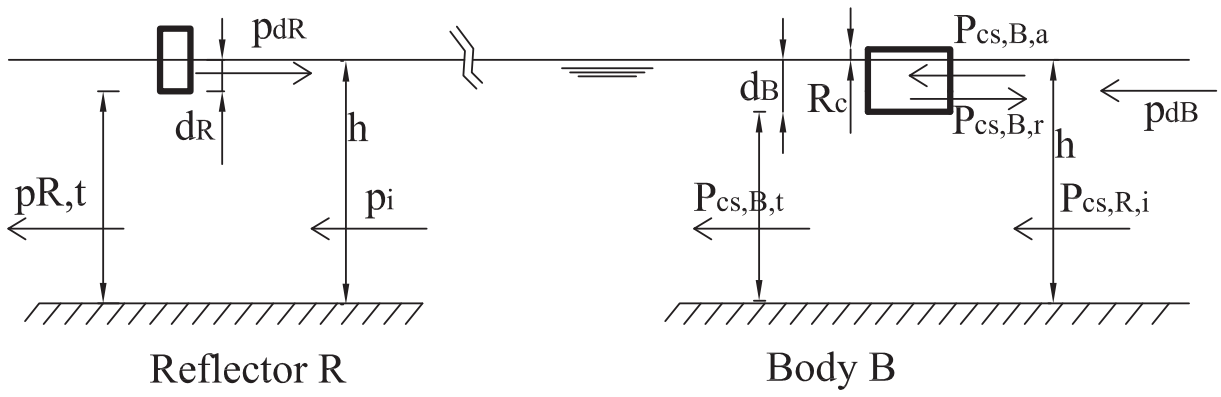

Fig. 7. Definition sketch of reflection on and transmission under the wave reflector and reflection on, transmission under and absorption by the main body – cross section.

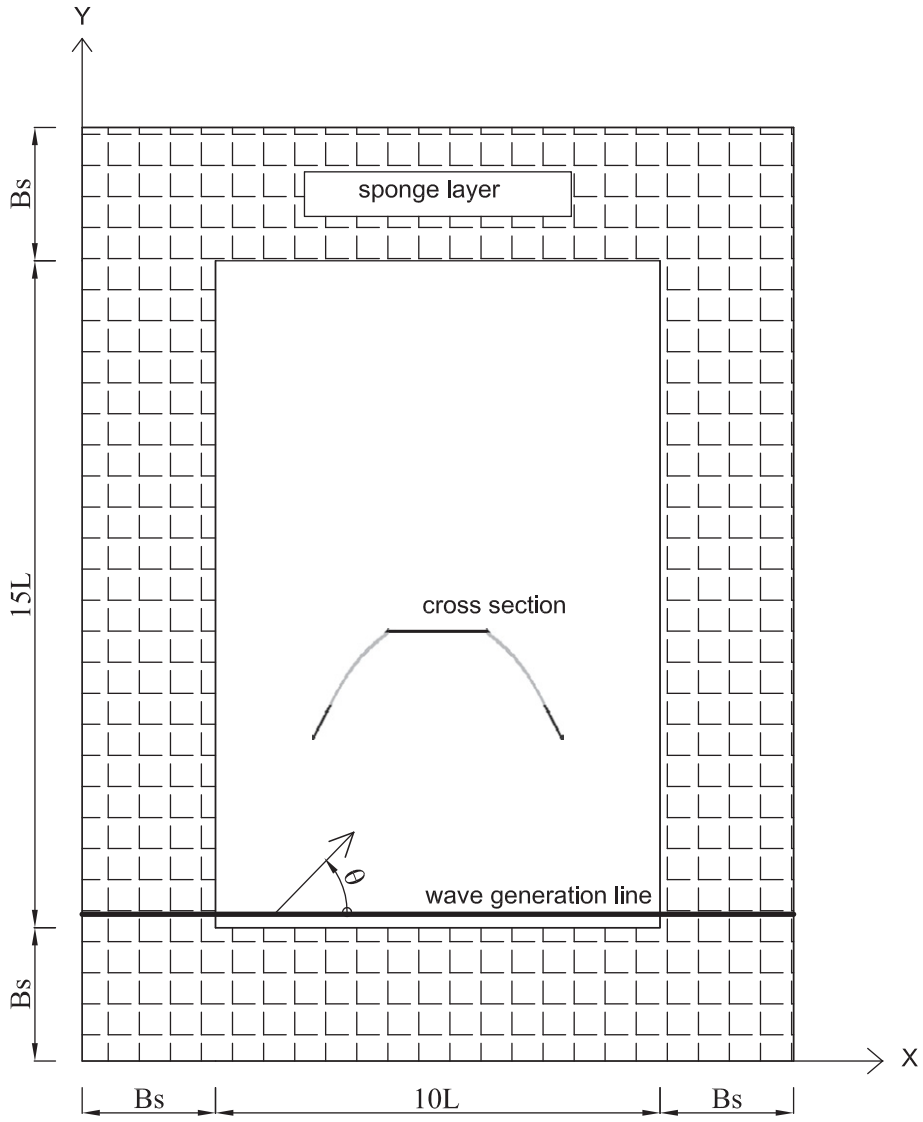

Fig. 8. Definition sketch of wave basin with wave reflectors in plan view for generation of unidirectional waves.

a draft of respectively 6 m and 8 m, are implemented in a wave basin as shown in Fig. 10. Wave propagation next to the reflector parts is prevented by the side walls of the wave basin.

By measuring the wave heights behind the wave reflector parts, the amounts of transmission under both reflector parts are determined. The combination of absorption coefficients which result in an accuracy of 5% on the amounts of transmission (Fig. 9) is selected. The absorption coefficients increase with increasing wave period, as the amount of reflection decreases (Table 2) and the amount of transmission increases (Fig. 9). Note that any possible future changes in reflector geometry can be easily taken into account using the developed methodology to implement the wave reflectors in MILDwave.

Table 2
Efficiency of wave reflectors for wave situations in the North Sea [4].

H_s m	T_p s	η_R^{target} %
1	5.6	185
2	7.0	145
3	8.4	124
4	9.8	120
5	11.2	115

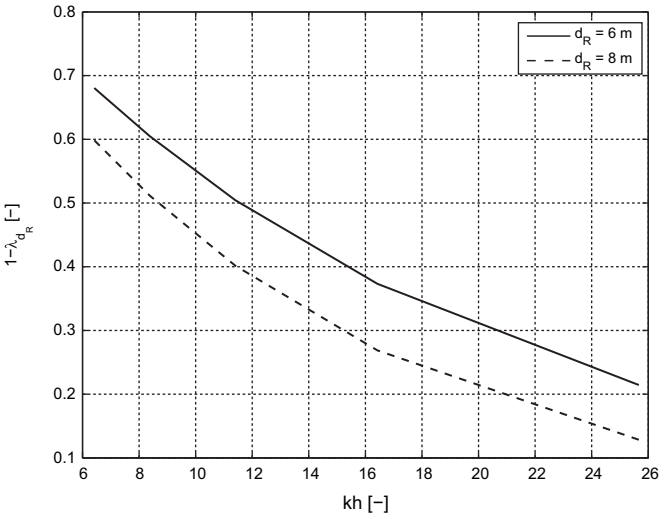

Fig. 9. Ratio between transmitted wave power under the wave reflector $p_{R,t}$ and incident wave power p_i as a function of kh for a reflector draft $d_R = 6$ m and $d_R = 8$ m.

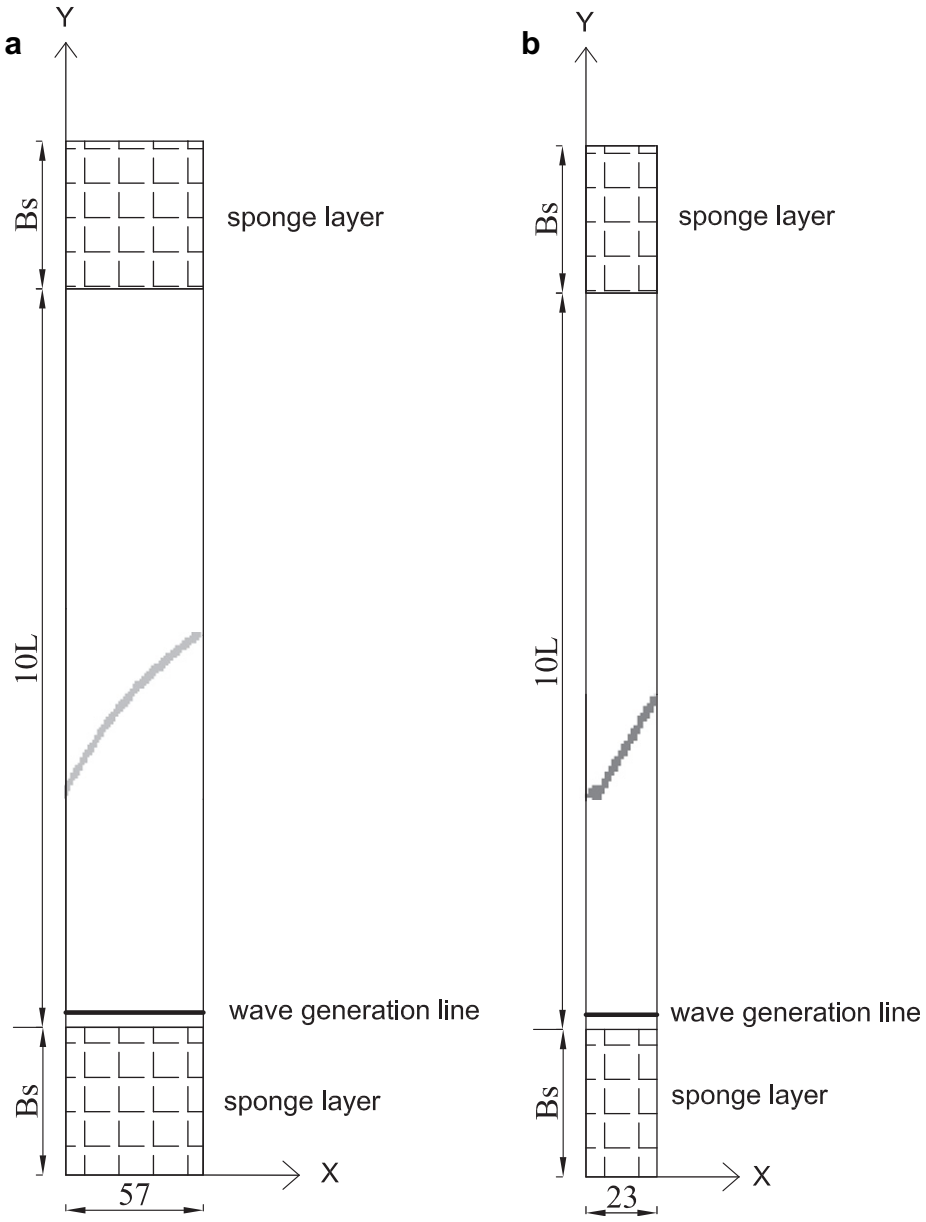

Fig. 10. Definition sketch of wave basin with wave reflector parts with draft (a) $d_R = 8$ m and (b) $d_R = 6$ m – dimensions in m.

3.2.2. Implementation of the main body

The main body converts potential energy into electricity by capturing the water volume of overtopped waves in a reservoir above mean sea level from which the water passes back to the sea through low head hydro turbines which drive permanent magnet generators. Consequently the main body absorbs a specific amount of wave power, $P_{cs,\,B,\,a}$ (W), which can be determined with equation (21) [2]:

$$P_{cs,B,a} = qR_c g\rho W_B \tag{21}$$

with the crest freeboard R_c, the overtopping rate q and the width of the ramp W_B, which is equal to 100 m.

Based on previous simulations the optimal relative floating level, R_c/H_s, is approximately 0.7–0.8 for electrical power generation [28]. In this work the absorbed wave power (defined as the power of the water flow overtopping the ramp) is studied instead of the electrical power. To optimize the concept of the Wave Dragon WEC for maximum power absorption it seems reasonable to use a lower value of R_c/H_s. A value of 0.5 has been used to estimate the absorbed power.

The overtopping rate q, modified by λ_{d_B}, is given by equation (22) [28]:

$$q = q_N \lambda_{d_B} \sqrt{gH_s^3} \tag{22}$$

where q_N is the non-dimensional overtopping rate [28]:

$$q_N = 0.4\exp^{-3.2R_c/H_s} \tag{23}$$

Not all wave power in the cross section $P_{cs,\,R,\,i}$ is absorbed by the main body. Again it is assumed that all wave power below the draft of the main body d_B is transmitted (Fig. 7). The transmitted wave power under the main body $P_{cs,B,t}$ (W) is given by $P_{cs,B,t} = P_{cs,R,i} - P_{d_B} = P_{cs,R,i}(1 - P_{d_B}/P_{cs,R,i}) = \eta_R^{\text{target}} P_{cs,\,i}(1 - \lambda_{d_B})$. The remaining wave power $P_{cs,B,r}$ (W) is reflected. The calculated ratios

Table 3
Dimensionless amounts of absorbed wave power, $P_{cs,B,a}$, and transmitted wave power under the main body, $P_{cs,B,t}$, for wave situations in the North Sea.

H_s m	T_p s	$\frac{P_{cs,B,a}}{P_{cs,R,i}}$ [−]	$\frac{P_{cs,B,t}}{P_{cs,R,i}} = 1 - \lambda_{d_B}$ [−]
1	5.6	0.28	0.02
2	7.0	0.36	0.09
3	8.4	0.38	0.19
4	9.8	0.33	0.31
5	11.2	0.29	0.42

between the absorbed wave power $P_{cs,B,a}$, respectively the transmitted wave power $P_{cs,\,B,\,t}$ and the wave power in front of the main body $P_{cs,\,R,\,i}$ are given in Table 3. These ratios are used to implement the main body in MILDwave with the sponge layer technique.

In MILDwave the shape of the main body in plan view is simplified to a rectangular body with a width W_B equal to the distance between the wave reflectors in the cross section (here $W_B = 100$ m) and a length equal to the length of the reservoir (=45 m), as indicated on Fig. 11.

The absorption, reflection and transmission characteristics of the main body are tuned in a numerical wave basin with a width equal to the width of the rectangular body W_B as explained in Section 2.2. The test set-up is shown in Fig. 12.

The main body is divided into 15 strips, each with a different value of S. The values of the absorption coefficients of the cells of the main body, to obtain the desired amounts of absorption and transmission (Table 3), are determined through an iterative approach. The surface elevations are measured by an array of three wave gauges, installed approximately one wave length in front of the main body and one wave gauge behind the main body, to determine the amounts of reflection on and transmission through the main body. The measured time series are divided into subseries with a duration of 204.8 s corresponding to a spectral resolution of $\Delta f = 0.00488$ Hz. A taper window and an overlap of 20% are used for smoother and statistically more significant spectral estimates. The frequency range is confined between $0.75\bar{f}$ and $2\bar{f}$ which covers 94% of the total energy. The ratio between the absorbed wave power $P_{cs,\,B,\,a}$ and the total wave power in the cross section $P_{cs,\,R,\,i}$ is calculated with equation (18), $P_{cs,B,a}/P_{cs,R,i} = (P_{cs,B,a}/\eta_R^{\text{target}} P_{cs,i}) = 1 - K_r^2 - K_t^2$.

The combination of absorption coefficients S which result in an accuracy of 5% on the amounts of absorption and transmission as given in Table 3, is selected. Again the absorption coefficients increase with increasing wave period.

3.3. Wake effect

By assembling both structural elements (reflectors and main body), which are tuned in Section 3.2, a Wave Dragon WEC is implemented in a wave basin in MILDwave, as shown in Fig. 13. As the Wave Dragon WEC is floating, the WEC will move and may disturb the wave pattern. However, open air-chambers under the main body with a pressurized air system are not only adjusting the floating height, but are also reducing the movements of the Wave Dragon WEC. Furthermore its size makes the Wave Dragon WEC more stable. In Frigaard et al. [5] it is stated that the movements of the 1:4.5 prototype scale model of the Wave Dragon WEC are smaller than expected from the laboratory measurements. In this work the Wave Dragon WEC is assumed to be restrained and consequently movements are neglected. The same assumption has been made in Nielsen and Kofoed [3].

The disturbance coefficients $K_d = (H_{s,d}/H_{s,i})$, where $H_{s,\,d}$ is the measured disturbed significant wave height, in a wave basin with a single Wave Dragon WEC for long-crested (head on) waves with a significant wave height of 1 m and a peak wave period of 5.6 s are shown in Fig. 13. Only the useful domain without sponge layers is shown. The Wave Dragon WEC is indicated in black.

The disturbance coefficients in a longitudinal section at $x = 1500$ m and in five lateral sections at respectively $y = 750$ m, 1750 m, 3750 m, 6750 m and 8750 m (all sections are indicated on Fig. 13) are shown in Figs. 14 and 15. Note that the longitudinal section starts right behind the Wave Dragon WEC at $y = 750$ m (Fig. 14). Immediately behind the Wave Dragon WEC a large decrease of the disturbed significant wave height is seen, while a gradual redistribution occurs behind the Wave Dragon WEC due to diffraction around the WEC. The large wave height decrease right behind the Wave Dragon WEC does not imply that all energy is absorbed. For irregular long-crested waves with $H_s = 1$ m and $T_p = 5.6$ s approximately 70% of the wave power in front of the main body $P_{cs,\,R,\,i}$ is reflected (28% is absorbed and 2% is transmitted as indicated in Table 3).

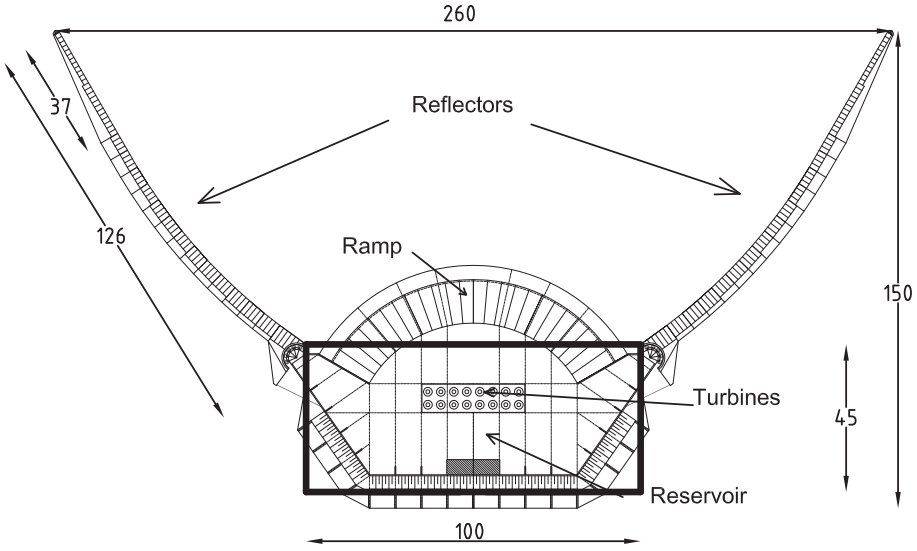

Fig. 11. Simplification of the main body of a Wave Dragon WEC – dimensions in m.

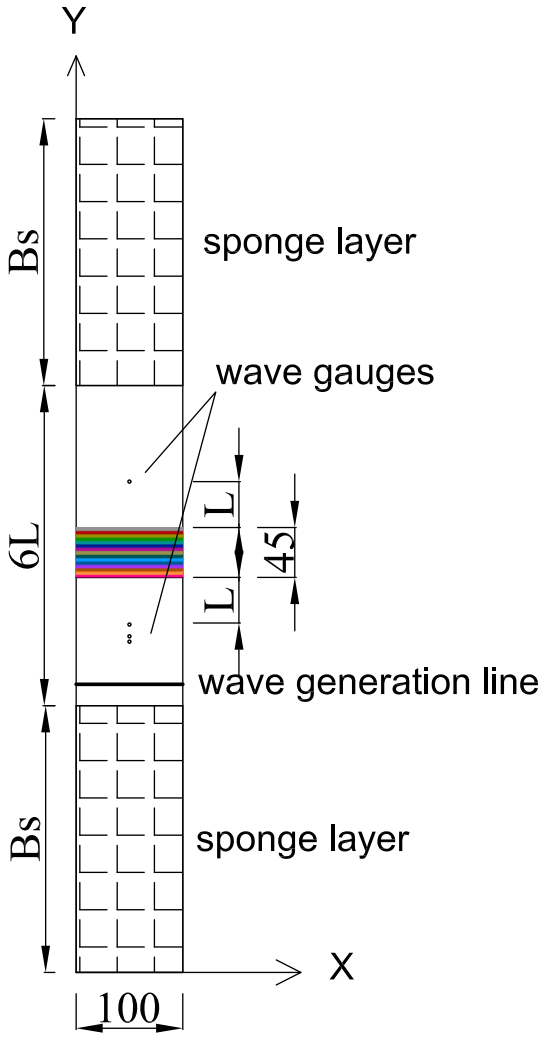

Fig. 12. Definition sketch of wave basin with main body in plan view for generation of unidirectional waves – dimensions in m.

For irregular long-crested waves with $H_s = 1$ m and $T_p = 5.6$ s, the Wave Dragon WEC is absorbing $P_{cs,\ B,\ a} = 125$ kW $= P_{s,\ 1}$ (equation (21)). $P_{s,\ 1}$ is the power absorbed by a single Wave Dragon WEC in wave situation 1. The possible power absorbed by a second Wave Dragon WEC, installed behind the first Wave Dragon WEC between $x = 1370$ m and $x = 1630$ m, is estimated by calculating the average significant wave height in front of the second Wave Dragon WEC (Fig. 13). This average wave height and the incident peak wave period are used to estimate the overtopping rate and consequently the absorbed power $P_{cs,\ B,\ a}$ of the second Wave Dragon WEC with equation (21). It is assumed that the incident peak wave period remains unchanged in the simulation domain. When studying diffraction past the tip of a semi infinite breakwater or diffraction through a breakwater gap, a small change in peak wave period was observed [29]. A second Wave Dragon WEC installed right behind the first one at $y = 1750$ m, 3750 m, 6750 m and 8750 m would absorb respectively only $P_{cs,\ B,\ a} = 0.12\ P_{s,\ 1}$, $0.29\ P_{s,\ 1}$, $0.45\ P_{s,\ 1}$ and $0.50\ P_{s,\ 1}$. The average available wave power p_i in those sections is respectively 18%, 37%, 52% and 57% of the available wave power $p_i = 2.5$ kW/m (Table 1) in front of the first WEC. A second Wave Dragon WEC, installed 8 km behind the first one, would only absorb half of the power absorbed by the first Wave Dragon WEC. For this long-crested wave situation, a very large distance between the WECs is needed to have a sufficient redistribution behind the first

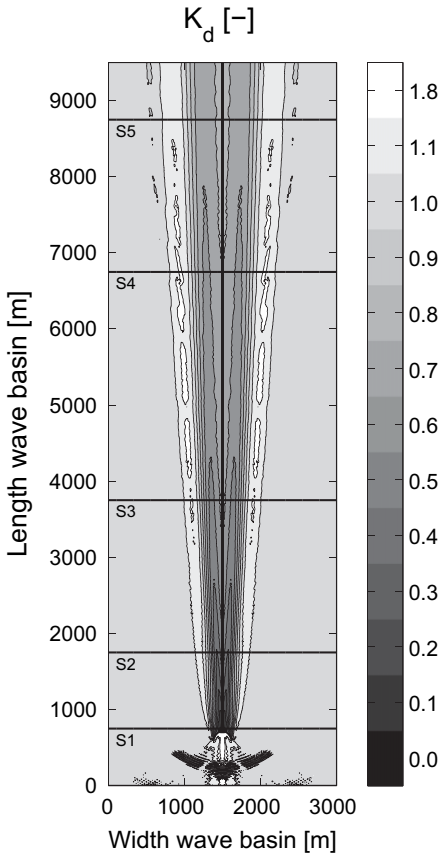

Fig. 13. Calculated disturbance coefficient K_d in a wave basin with a single Wave Dragon WEC for irregular long-crested waves (head on) with $H_s = 1$ m and $T_p = 5.6$ s.

WEC. One should keep in mind that so far only long-crested (no directional spreading) incident waves with $T_p = 5.6$ s have been considered. The wake behind a single Wave Dragon WEC in a short-crested sea with a mean wave direction of 90° and a directional width of respectively approximately 9° ($s_{max} = 75$) and 24° ($s_{max} = 10$) for the peak period ($T_p = 5.6$ s) is shown in Fig. 16(b) and (c). Furthermore the wake for irregular long-crested waves as given

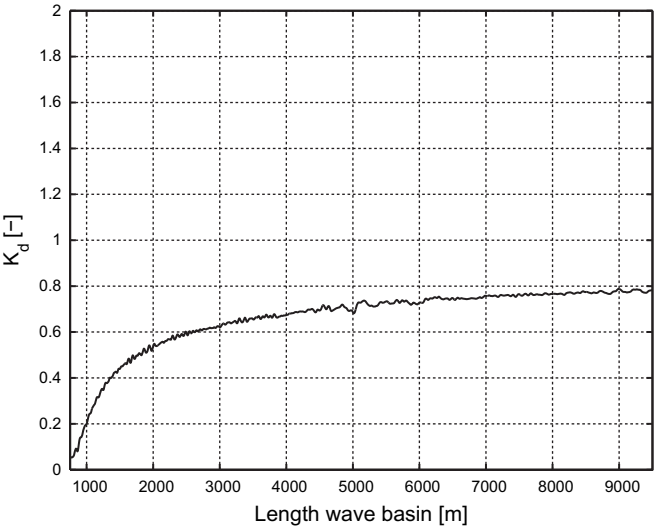

Fig. 14. Calculated disturbance coefficient K_d in a longitudinal section at $x = 1500$ m, as indicated on Fig. 13, shown only behind the Wave Dragon WEC.

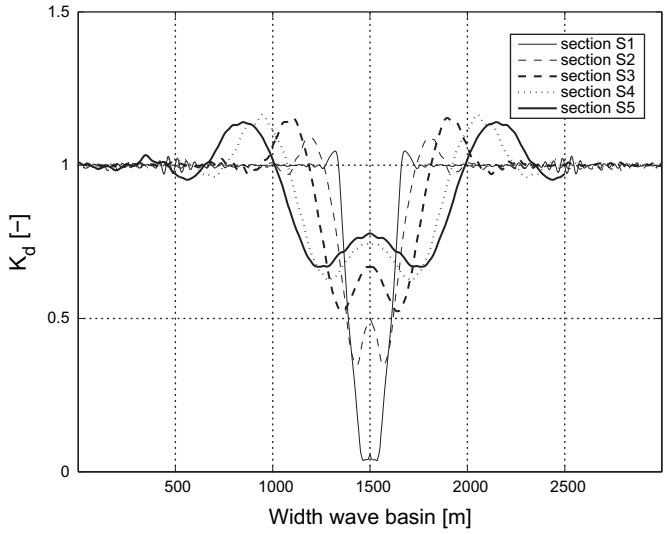

Fig. 15. Calculated disturbance coefficient K_d in lateral sections at y = respectively 750 m, 1750 m, 3750 m, 6750 m and 8750 m, as indicated on Fig. 13.

in Fig. 13 is shown in more detail (500 m $\leq x \leq$ 2500 m and 0 m $\leq y \leq$ 4500 m) in Fig. 16(a). As expected, the wake length shortens with increasing directional spreading due to a faster redistribution behind the WEC. A wider wake is observed when short-crested waves are generated. Furthermore, the small increase in wave height as seen at the edges of the wake in Fig. 16(a) disappears in a short-crested sea. Three lateral sections S1, S2 and S3 behind the Wave Dragon WEC are shown in Fig. 17 for the same wave conditions as considered in Fig. 16. The wave height decrease right behind the Wave Dragon WEC at $y = 750$ m is comparable for the three wave conditions. At $y = 1750$ m the effects of the directional spreading are clearly present. The remaining wave height behind the Wave Dragon WEC increases with increasing directional spreading. At $y = 3750$ m (3 km behind the WEC) the wave height is practically equal to the wave height in front of the WEC for short-crested waves with $s_{max} = 10$. A Wave Dragon WEC installed right behind the first one at $y = 1750$ m and 3750 m would absorb respectively $P_{cs,\,B,\,a} = 0.41\ P_{s,\,1}$ and $0.68\ P_{s,\,1}$ when $s_{max} = 75$ and $P_{cs,\,B,\,a} = 0.67\ P_{s,\,1}$ and $0.9\ P_{s,\,1}$ when $s_{max} = 10$ (equation (21)). In the case of long-crested waves and swell waves ($s_{max} = 75$) a second WEC installed 3 km behind the first WEC is absorbing less than 70% of the first WEC ($0.29\ P_{s,\,1}$ and $0.68\ P_{s,\,1}$, respectively). As in practice the available space to install a farm of WECs is rather small, a WEC in a second row should not be installed right behind a WEC in the first row. Therefore, in the next section a farm of five Wave Dragon WECs, installed in a staggered grid, is studied.

In the next sections only long-crested irregular waves are considered, as they cause the largest wake behind the WEC and consequently the largest impact on the neighbouring WECs in the farm. As a consequence the obtained results will be rather conservative. Furthermore no local wind generation is included in the model. Further research on these effects will be carried out to optimize the farm lay-out for short-crested waves.

4. Optimal lay-out of a farm of 5 Wave Dragon WECs

The power absorption of one Wave Dragon WEC affects the available wave power for the Wave Dragon WECs in its lee. The reduction of the available wave power depends on the distances between the Wave Dragon WECs in a farm, the incident wave climate (transmission under main body and wave reflectors increases for increasing wave period and wave height) and the directional spreading of the incident waves. As for long-crested waves a large distance between two Wave Dragon WECs, installed right behind each other, is needed to have an acceptable absorption of the second Wave Dragon WEC, the latter Wave Dragon WEC will be shifted, resulting in a staggered grid (Fig. 18). The distances between the WECs in a farm should be as small as possible to reduce the use of available sea area and also the cost of the farm. On the other hand a minimal distance of 260 m is needed between two adjacent Wave Dragon WECs to prevent collision, as the rotation of

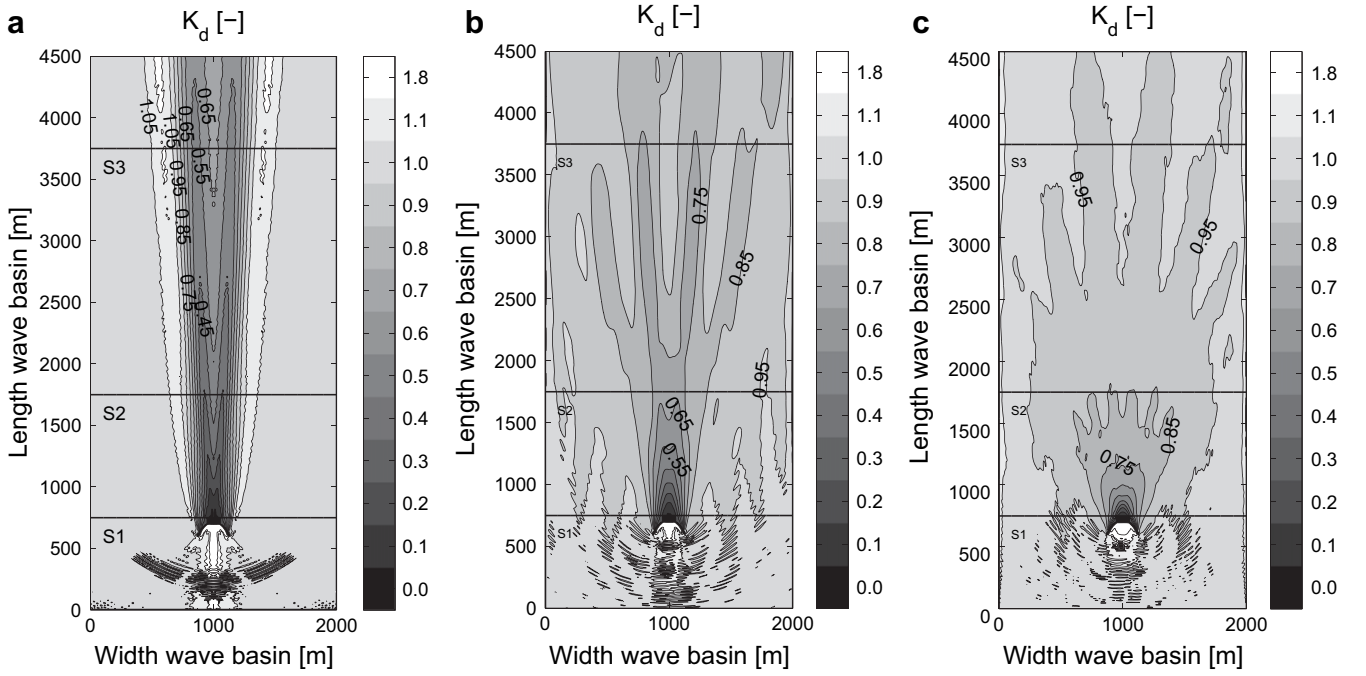

Fig. 16. Calculated disturbance coefficient K_d in a wave basin with a single Wave Dragon WEC for irregular (a) long-crested waves (head on) with $T_p = 5.6$ s (identical to Fig. 13) and short-crested waves (head on) with $T_p = 5.6$ s and s_{max} of respectively (b) 75 and (c) 10.

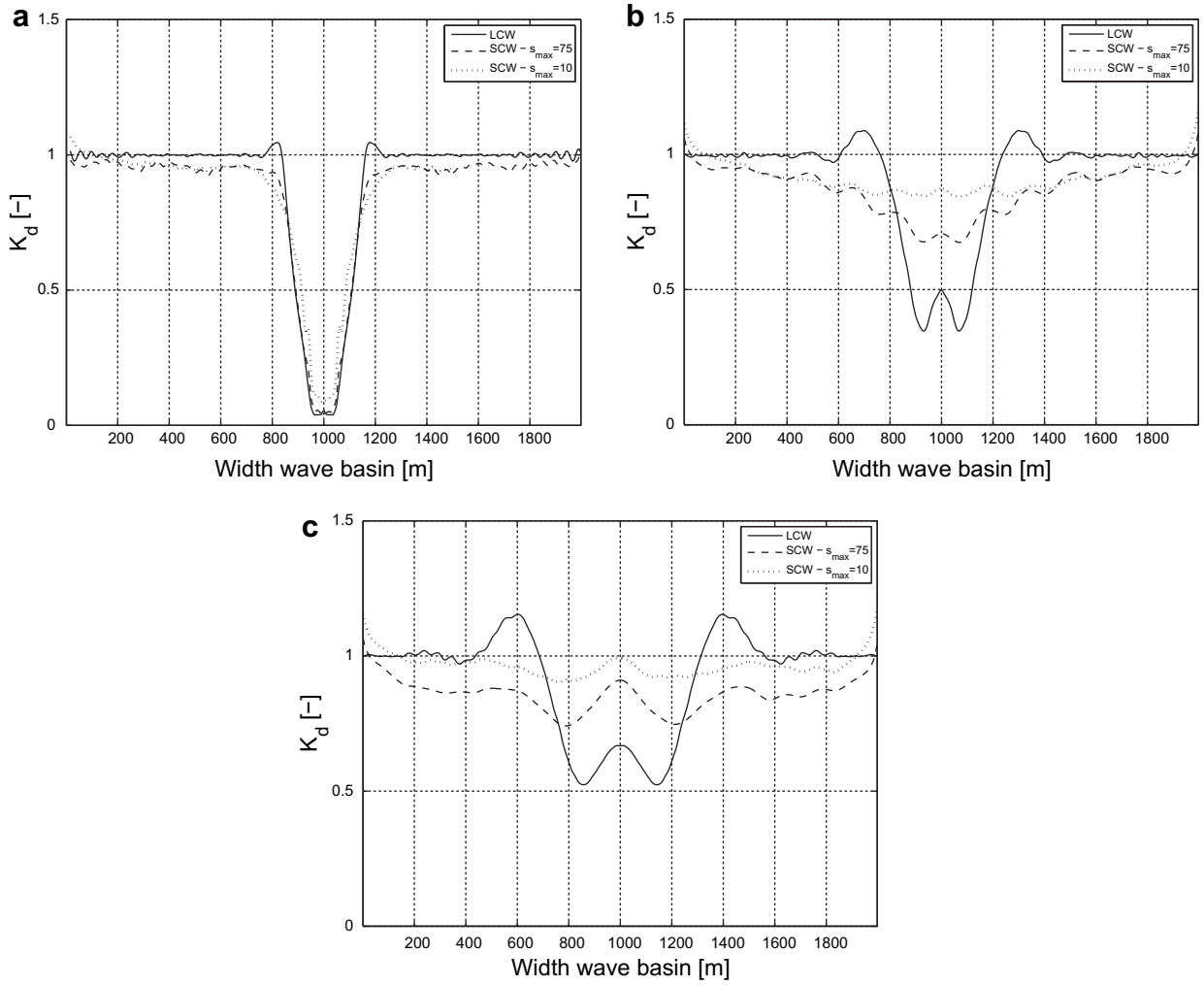

Fig. 17. Calculated disturbance coefficient K_d in lateral sections at $y =$ respectively (a) 750 m, (b) 1750 m and (c) 3750 m as indicated on Fig. 16 in a wave basin with a single Wave Dragon WEC for irregular long-crested waves (LCW) with $T_p = 5.6$ s and short-crested waves (SCW) with $T_p = 5.6$ s and s_{max} of respectively 75 and 10.

the Wave Dragon WEC is assumed to be restricted to $\pm 60^{\circ}$ by its anchor system [30]. Five Wave Dragon WECs (Fig. 18) installed in a staggered grid with an in-between distance of respectively D, $2D$ and $3D$, with D the distance between the tips of the wave reflectors of a single WEC (=260 m), are studied for the wave situation with the highest frequency of occurrence (Table 1). The optimal lay-out for this wave situation will be defined and the absorption of five Wave Dragon WECs installed in the selected farm lay-out will be calculated in Section 5 for the remaining wave situations in the North Sea (Table 1).

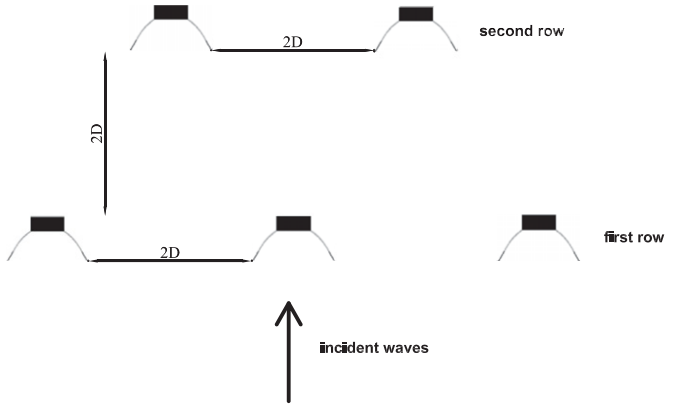

Fig. 18. 5 Wave Dragon WECs with an in-between distance $2D$ installed in a staggered grid.

First only one row with 3 Wave Dragon WECs, each absorbing $P_{cs,\,B,\,a} = 125$ kW $= P_{s,\,1}$ is installed in a wave basin as shown in Fig. 19. The length and the width of the wave basin are adapted for each lay-out to obtain a sufficiently large domain. The resulting calculated disturbance coefficients for an in-between distance of respectively D, $2D$ and $3D$ are shown in Fig. 19. Again only the useful domain without sponge layers is shown. Furthermore the positions of Wave Dragon WECs in the second row are indicated. The remaining wave height behind the first row determines the absorbed power of the WECs in the second row. On the positions of the Wave Dragon WECs in the second row the average available wave power p_i is decreased with 8% for an in-between distance of D and increased with respectively 6% and 1% for an in-between distance of respectively $2D$ and $3D$ compared to the available wave power in front of the first row ($p_i = 2.5$ kW/m). This small increase of wave power will not occur when short-crested waves are generated, as explained in Section 3.3. The directional spreading will smooth out the latter effect. It is clear that the available wave power for the second row p_i is approximately equal to the available

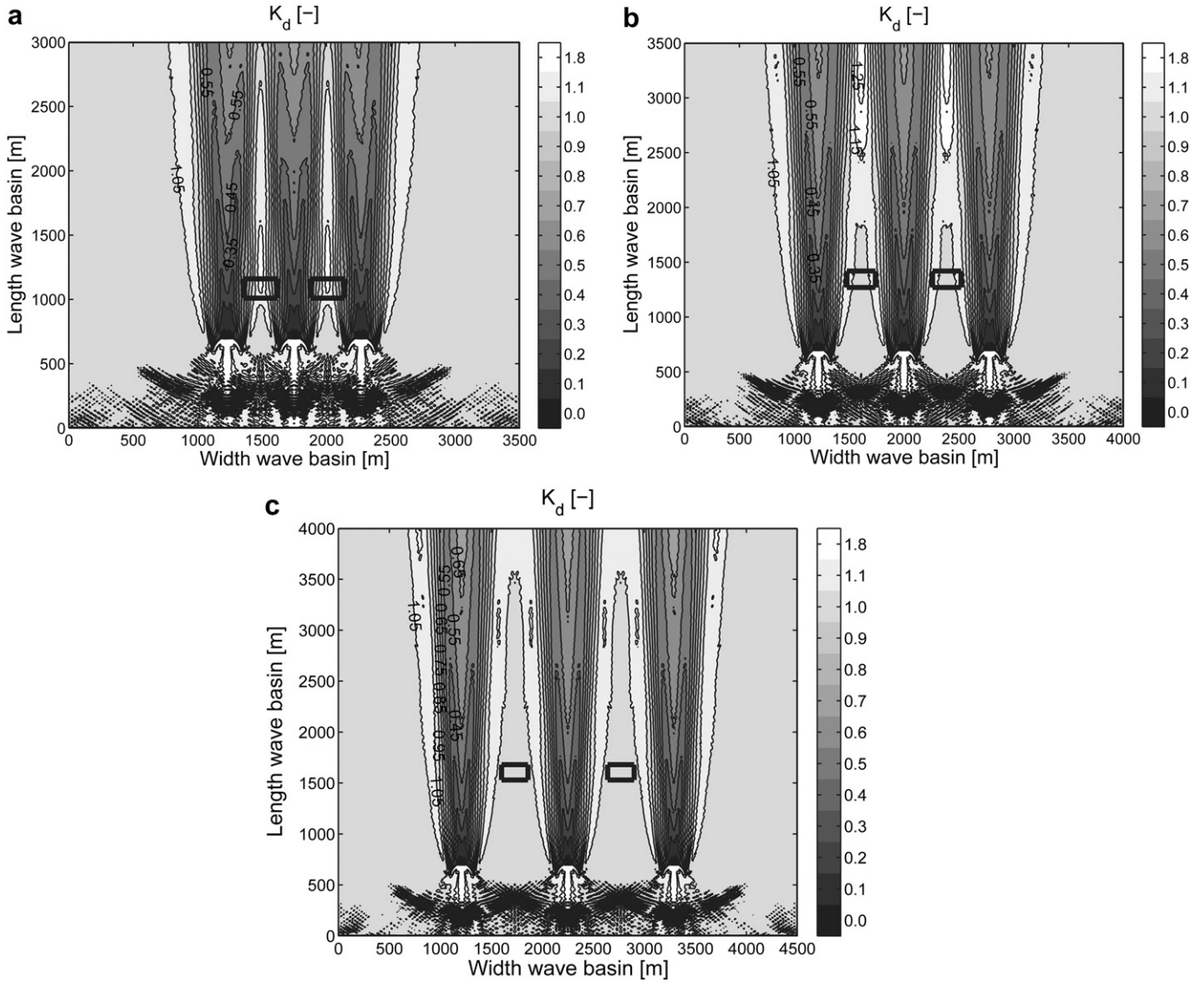

Fig. 19. Calculated disturbance coefficient K_d in a wave basin with 3 Wave Dragon WECs with an in-between distance of respectively (a) D, (b) $2D$ and (c) $3D$, with $D = 260$ m, for irregular long-crested waves (head on) with $T_p = 5.6$ s.

wave power for the first row ($p_i = 2.5$ kW/m) for each in-between distance. A single Wave Dragon WEC in the second row will absorb respectively $P_{cs,\,B,\,a} = 0.88\,P_{s,\,1}$, $1.07\,P_{s,\,1}$ and $P_{s,\,1}$, using equation (21), when the WECs are installed in a staggered grid with an in-between distance of respectively D, $2D$ and $3D$. The difference in power absorption between a lay-out of 5 WECs with an in-between distance of respectively $2D$ and $3D$ is very small. The total power absorption is approximately equal to $5\,P_{s,\,1}$.

Further both rows are installed in a wave basin as shown in Fig. 20. The Wave Dragon WECs in the second row have been tuned as described in Section 3. Waves are simulated during 4400 s (time step = 0.1 s) in a domain of 5000 cells (width) × 8000 cells (length) which resulted in a computational time of 64 h (Intel Core 2 CPU @ 2.40 GHz - 3 GB RAM). The calculated disturbance coefficients for the staggered grids with an in-between distance of respectively D, $2D$ and $3D$ are shown in Fig. 20. The disturbance coefficients in a cross section right behind and 4 km behind the latter grids are compared in Fig. 21.

Behind each grid a large wave power decrease is observed. When the in-between distance is increasing, more wave power is propagating between the WECs in the farm (Fig. 21). The power that WECs installed in a third row (identical to the first row) would absorb, is given in Table 4. For all grids, the absorbed wave power of the WECs in the third row is smaller than $0.2\,P_{s,\,1}$. A very large in-between distance is needed to have sufficient wave power on a third row, which is not economic. It is clear that the optimal lay-out consists of 2 rows, as the wave power absorption in a third row is too small. The lay-out with an in-between distance of $2D$ is selected for further investigation, as the required sea area and cost will be smaller compared to a staggered grid with an in-between distance of $3D$. Furthermore its power absorption is higher than the power absorbed by Wave Dragon WECs installed in a staggered grid with an in-between distance of D.

5. Absorption of the selected farm lay-out

The absorbed wave power of 5 Wave Dragon WECs, installed in a staggered grid with an in-between distance of $2D$ equals approximately $5\,P_{s,\,1}$ when irregular long-crested waves with $H_s = 1$ m and $T_p = 5.6$ s are generated. In this section the absorption

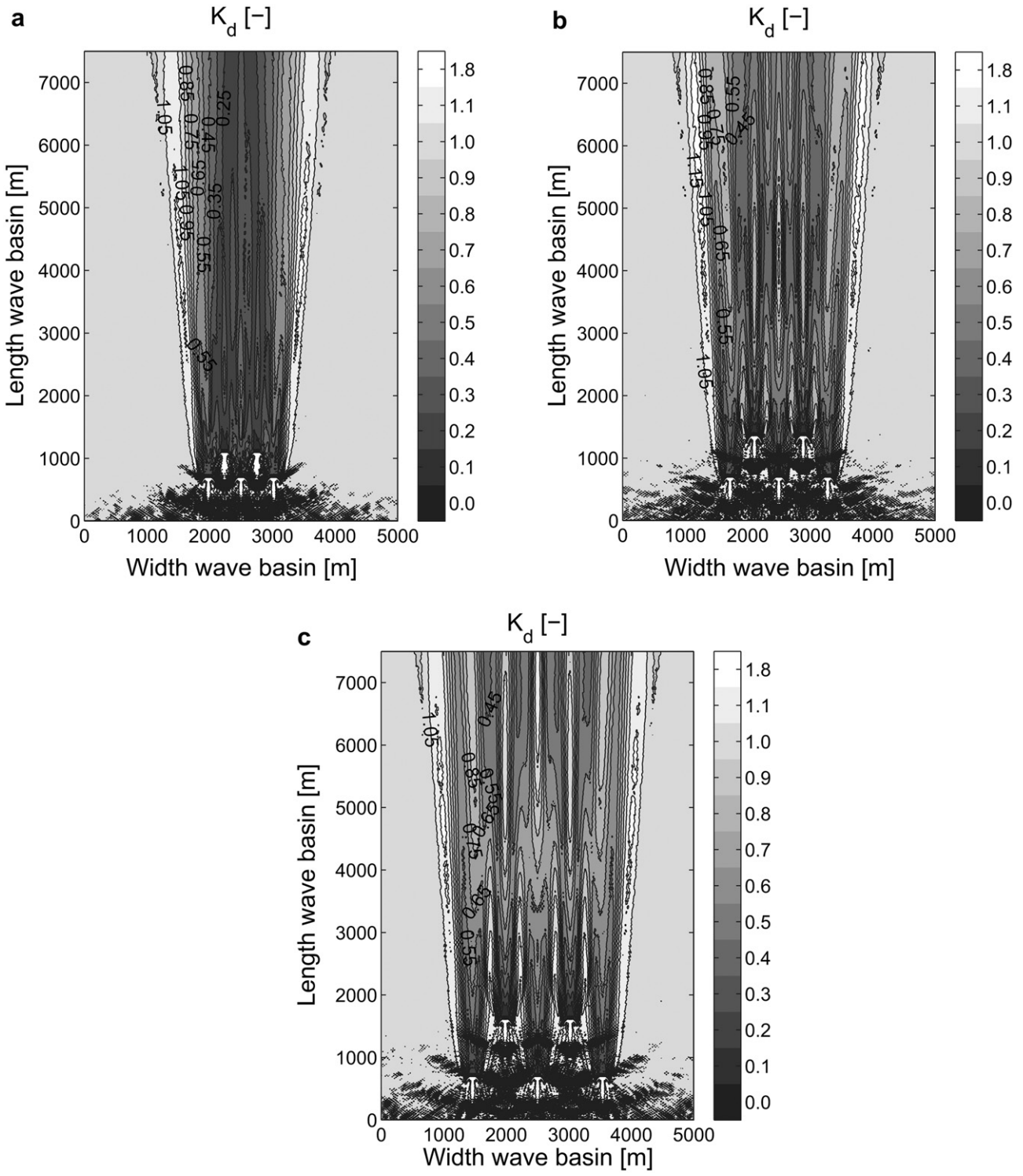

Fig. 20. Calculated disturbance coefficient K_d in a wave basin with 5 Wave Dragon WECs with an in-between distance of respectively (a) D, (b) $2D$ and (c) $3D$, with $D = 260$ m, for irregular long-crested waves (head on) with $T_p = 5.6$ s.

of the selected farm in the remaining wave situations in the North Sea (Table 1) is derived. The disturbance coefficients are calculated in a basin with only the first row of WECs installed (Fig. 22) for the remaining irregular long-crested waves with respectively $T_p = 7$ s, 8.4 s, 9.8 s and 11.2 s. A wider shadow zone and a smaller wave height decrease behind each Wave Dragon WEC is observed for higher peak periods. The smaller wave height decrease is caused by the larger transmission (Table 3 and Fig. 9).

The wave power absorbed by a Wave Dragon WEC in the first, respectively second row for the different wave situations is given in Fig. 23. The wave power absorption of the Wave Dragon WECs in the second row is approximately equal to the absorption of the WECs in the first row for all wave situations. Note that the slightly higher absorption of the WECs in the second row is caused by the small wave height increase at the edges of the wake of a single Wave Dragon WEC for irregular long-crested waves. By installing the WECs in a staggered grid with an in-between distance of $2D$, the mean wave power in front of the second row is not affected. A farm of five Wave Dragon WECs, installed in a staggered grid with an in-between distance of 520 m, will absorb 5 times more than a single

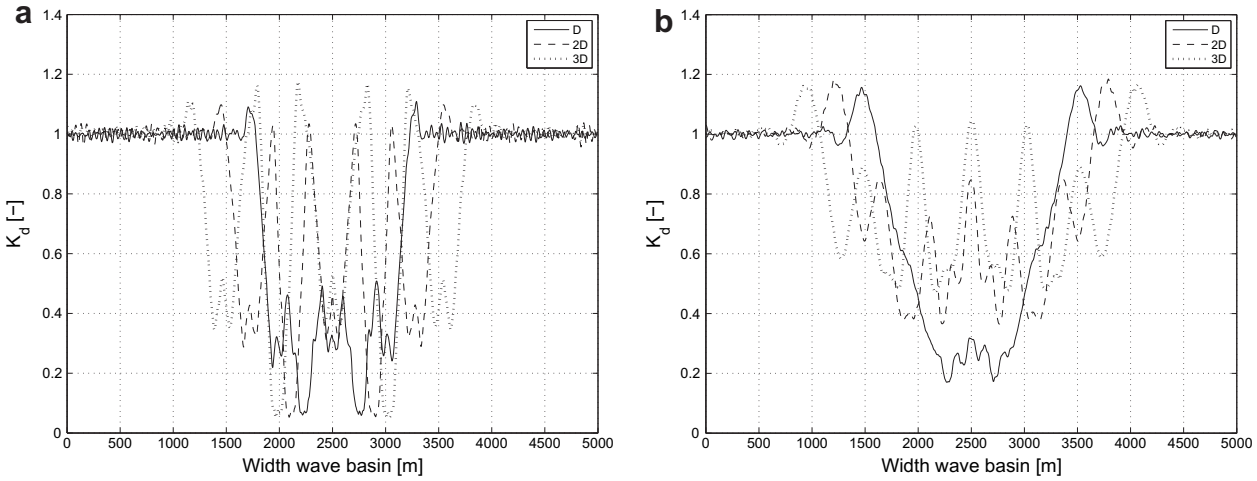

Fig. 21. Calculated disturbance coefficient K_d in two cross sections, (a) immediately behind and (b) 4 km behind the farm lay-outs from Fig. 20.

Table 4
Absorbed wave power of WECs [multiple of $P_{s,1}$] installed in a third row behind the farm with 5 WECs.

In-between distance	Wave Dragon 1	Wave Dragon 2	Wave Dragon 3
D	0.09	0.06	0.09
$2D$	0.16	0.17	0.16
$3D$	0.18	0.19	0.18

Wave Dragon WEC in each wave situation. The latter result can be easily extended for a wider farm consisting of two rows of Wave Dragon WECs installed in a staggered grid. WECs installed in a third row would absorb respectively approximately 0.17 $P_{s,1}$ (Table 4), 0.33 $P_{s,2}$, 0.54 $P_{s,3}$, 0.67 $P_{s,4}$, 0.82 $P_{s,5}$ for $T_p = 5.6$ s, 7 s, 8.4 s, 9.8 s and 11.2 s. $P_{s,i}$ is the power absorbed by a single WEC in the considered wave situation i ($i = 1, 2, 3, 4, 5$). 68% of the time the absorption of a WEC in a third row is smaller than 50% of the absorption of a WEC in the first two rows which makes a third row of converters not advantageously. When short-crested waves are dominating a faster redistribution was observed (Fig. 16). The installation of a third row could be interesting in a short-crested sea.

In this work an optimal lay-out has been selected for the wave situation with the highest frequency of occurrence. As an alternative the wave situation which contributes most to the mean wave power (p_i multiplied with its frequency of occurrence), which is the wave situation with $H_s = 5$ m and $T_p = 11.2$ s, could be considered. This approach will result in the same optimal lay-out. Note that in this work only head on waves have been studied. To calculate the yearly absorption other mean wave directions should be taken into account [31].

6. Conclusions

In this paper a farm of Wave Dragon WECs has been studied in the time-dependent mild-slope equation model MILDwave. A Wave Dragon WEC has been implemented as a porous structure with the same reflection, absorption and transmission characteristics as obtained for the prototype by using the sponge layer technique. The tuning of the Wave Dragon WEC for the North Sea wave climate has been described in detail for the wave reflectors and for the main body separately. By assembling the tuned wave reflectors and main body, a Wave Dragon WEC has been implemented in MILDwave.

The wake effects in the lee of a single Wave Dragon WEC have been calculated. For irregular long-crested head on waves a large decrease of wave power is observed behind the Wave Dragon WEC. The shadow zone behind the WEC is gradually filled up due to diffraction effects. The available wave power 8 km behind the WEC is only 57% of the generated wave power ($H_s = 1$ m and $T_p = 5.6$ s). For short-crested waves a faster wave redistribution is observed. The available wave power 3 km behind the WEC is approximately equal to the incident wave power for short-crested wave with $s_{max} = 10$ ($H_s = 1$ m and $T_p = 5.6$ s). When installing multiple WECs in a farm, the placing of a WEC in a second row right behind a WEC in the first row should be avoided. A staggered grid lay-out is preferred.

The wave height reduction in and around a farm of five Wave Dragon WECs installed in a staggered grid (respectively three and two Wave Dragon WECs installed in a first and second row), with an in-between distance of respectively D, $2D$ and $3D$ (D = distance between the tips of the wave reflectors of a single WEC), has been modelled for the North Sea wave situation with the highest frequency of occurrence. The difference in power absorption between the grids with an in-between distance of $2D$ and $3D$ is very small and the wave height reduction behind these grids is too large to make installation of an additional row commercially viable. A lay-out with an in-between distance of $2D$ has been selected as the optimal farm lay-out for the latter wave situation, taking cost and spatial considerations into account. Five Wave Dragon WECs installed in a staggered grid with an in-between distance of $2D$ will produce 5 times more than a single Wave Dragon WEC in a North Sea wave climate, as the incident wave power for the second row is not affected by the first row. In this farm study no directional spreading and local wind generation is taken into account. Furthermore, only head on waves have been considered. Further research will focus on the identification of the effect of directional spreading, mean incident wave direction and local wind generation on the wake behind multiple Wave Dragon WECs.

Acknowledgements

Research funded by Ph.D. grant of the Institute for the Promotion of Innovation through Science and Technology in Flanders (IWT-Vlaanderen), Belgium. The authors would like to thank Tom Versluys for his contribution in optimising the code and developing a graphical interface. Robby Caspeele and Sam Pecqueur are acknowledged for their assistance in extending the

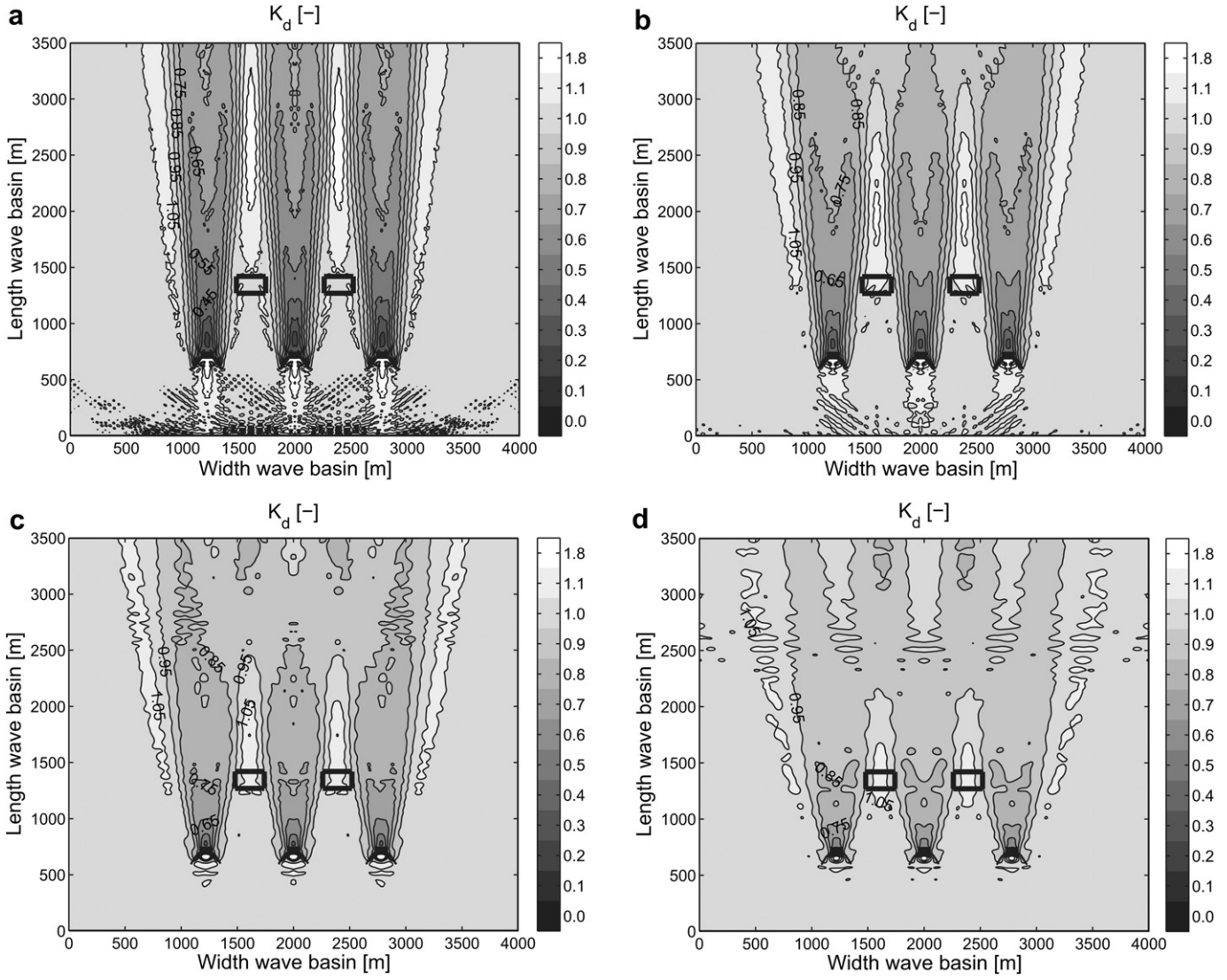

Fig. 22. Calculated disturbance coefficient K_d in a wave basin with 3 Wave Dragon WECs with an in-between distance of 2D, with $D = 260$ m, for irregular long-crested waves (head on) with respectively (a) $H_s = 2$ m and $T_p = 7$ s, (b) $H_s = 3$ m and $T_p = 8.4$ s, (c) $H_s = 4$ m and $T_p = 9.8$ s and (d) $H_s = 5$ m and $T_p = 11.2$ s.

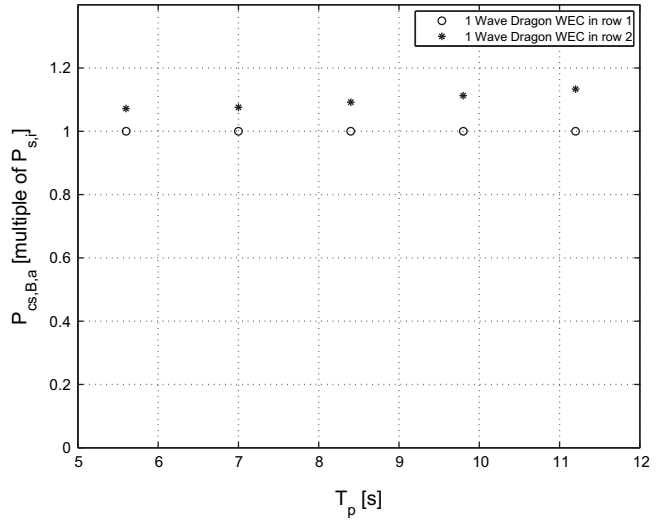

Fig. 23. Wave power absorbed by 1 Wave Dragon WEC in the first respectively second row of the optimal farm lay-out for wave situations in the North Sea.

wave generation technique. Wave Dragon ApS. (WD-MW FP6 EU project) and James Tedd (Aalborg University) are gratefully acknowledged for providing the data on which this study is based.

References

[1] Tedd J, Kofoed JP, Friis-Madsen E. Renovation of the Wave Dragon Nissum Bredning prototype. In: Proceedings of the 16 th ISOPE conference, San Francisco; 2006.
[2] Kofoed JP. Wave overtopping of marine structures – utilization of wave energy, Ph.D. thesis. Hydraulics and Coastal Engineering Laboratory, Department of Civil Engineering, Aalborg University; 2002.
[3] Nielsen A, Kofoed JP. The Wave Dragon – evaluation of a wave energy converter, master's thesis. Hydraulics and Coastal Engineering Laboratory, Department of Civil Engineering, Aalborg University; 1997.
[4] Kramer M. Frigaard P. Efficient wave energy amplification with wave reflectors, Proceedings of the 9 th ISOPE conference; 2002.
[5] Frigaard P, Kofoed JP, Rasmussen M.R. Overtopping measurements on the Wave Dragon Nissum Bredning prototype. In: Proceedings of the 11 th ISOPE conference, Toulon; 2004.
[6] Martinelli L, Frigaard P. The Wave Dragon: 3D overtopping tests on a floating model. Low-pressure turbine and control equipment for wave energy converters (Wave Dragon), Tech. rep. Hydraulics and Coastal Engineering Laboratory, Aalborg University; 1999.

[7] Knapp W, Holmen E, Schilling R. Considerations for water turbines to be used in wave energy converters, Proceedings of the 4 th European Wave Energy conference, Aalborg; 2000.
[8] Frigaard P, Kofoed JP, Knapp W. Wave Dragon. Wave power plant using low-head turbines, Hidroenergia, Falkenberg.
[9] Kofoed JP, Frigaard P, Friis-Madsen E, Sørensen HC. Prototype testing of the wave energy converter Wave Dragon. Renewable Energy 2006;31:181–9.
[10] Tedd J, Friis-Madsen E, Kofoed JP, Knapp W. 7.4 wave Dragon. In: Cruz J, editor. Ocean wave energy, current status and perspectives. Springer; 2008. p. 321–35.
[11] Spok, Wave Dragon 1: 4.5, Tech. rep., Spok; 2006.
[12] Radder AC, Dingemans MW. Canonical equations for almost periodic, weakly nonlinear gravity waves. Wave Motion 1985;7:473–85.
[13] Beels C, Troch P, De Backer G, Vantorre M, De Rouck J. Numerical implementation and sensitivity analysis of a wave energy converter in a time-dependent mild-slope equation model. Coastal Engineering, in press, doi:10.1016/j.coastaleng.2009.11.003.
[14] Booij N. A note on the accuracy of the mild-slope equation,. Coastal Engineering 1983;7:191–203.
[15] Lee C, Suh KD. Internal generation of waves for time-dependent mild-slope equations. Coastal Engineering 1998;34:35–57.
[16] Lee C, Kim G, Suh KD. Extended mild-slope equation for random waves. Coastal Engineering 2003;48:277–87.
[17] Liu Z, Frigaard P. Random seas, Tech. rep. Hydraulics and Coastal Engineering Laboratory, Aalborg University; 1997.
[18] Lee C, Yoon SB. Internal generation of waves on an arc in a rectangular grid system. Coastal Engineering 2007;54:357–68.
[19] Miles MD. A note on directional random wave synthesis by the single-summation method. Proceedings 23d IAHR Congress, Vol. C, Ottawa, ON, Canada, IAHR; 1989. 243–250.
[20] Mitsuyasu H, Tasai F, Suhara T, Mizuno S, Ohkusu M, Honda T, et al. Observations of the directional spectrum of ocean waves using a cloverleaf buoy. Journal of Physical Oceanography 1975;5:750–60.
[21] Goda Y, Suzuki Y. Computation of refraction and diffraction of sea waves with mitsuyasu's directional spectrum, Technical Note of Port and Harbor Research Institute 230; 1975.
[22] Kuik AJ, Vledder G, Holthuijsen LH. A method for the routine analysis of pitch and roll buoy wave data,. Journal of Physical Oceanography 1988;18:1020–34.
[23] Larsen J, Dancy H. Open boundaries in short wave simulations – a new approach. Coastal Engineering 1983;7:285–97.
[24] Brorsen M, Helm-Petersen J. On the reflection of short-crested waves in numerical models. In: Proceedings of the 26th International Conference on Coastal Engineering, Copenhagen; 1998. p. 394–407.
[25] Suh KD, Lee C, Park YH, Lee TH. Experimental verification of horizontal two-dimensional modified mild-slope equation model. Coastal Engineering 2001;44:1–12.
[26] Mansard EPD, Funke E.R. The measurement of incident and reflected spectra using a least squares method. In: Proceedings of the 17th International Conference on Coastal Engineering; 1;1980:154–72.
[27] Rugbjerg M, Nielsen K. Mapping of wave energy conditions in the Danish sector of the North Sea (in Danish: Kortlægning af bølgeenergiforhold i den danske del af Nordsøen). Danish Energy Agency/ ENERGISTYRELSEN J.no. 51191/97-0014. June 1999.
[28] Tedd J, Kofoed JP, Knapp W, Friis-Madsen E, Sørensen HC. Wave Dragon prototype wave power production. In: Proceedings of the World Renewable Energy Congress – IX, Florence; 2006.
[29] U.S. Army Corps of Engineers, Coastal Engineering Manual (CEM) – Part II: Coastal Hydrodynamics – Chapter II-7: Harbor Hydrodynamics; 2002.
[30] Tedd J, Kofoed JP, Friis-Madsen E, Christensen L. 7.5.5 wave Dragon. In: Cruz J, editor. Ocean wave energy, current status and perspectives. Springer; 2008. p. 371–82.
[31] Beels C. Optimization of the lay-out of a farm of wave energy converters in the North Sea. Analysis of wave power resources, wake effects, production and cost, Ph.D. thesis. Department of Civil Engineering, Ghent University; 2009.